



SPE 114164

Rock Typing — Keys to Understanding Productivity in Tight Gas Sands

J.A. Rushing, SPE, Anadarko Petroleum Corp., K.E. Newsham, SPE, Apache Corp., and T.A. Blasingame, SPE, Texas A&M University

Copyright 2008, Society of Petroleum Engineers

This paper was prepared for presentation at the 2008 SPE Unconventional Reservoirs Conference held in Keystone, Colorado, U.S.A., 10–12 February 2008.

This paper was selected for presentation by an SPE program committee following review of information contained in an abstract submitted by the author(s). Contents of the paper have not been reviewed by the Society of Petroleum Engineers and are subject to correction by the author(s). The material does not necessarily reflect any position of the Society of Petroleum Engineers, its officers, or members. Electronic reproduction, distribution, or storage of any part of this paper without the written consent of the Society of Petroleum Engineers is prohibited. Permission to reproduce in print is restricted to an abstract of not more than 300 words; illustrations may not be copied. The abstract must contain conspicuous acknowledgment of SPE copyright.

Abstract

This paper presents a work-flow process to describe and characterize tight gas sands. The ultimate objective of this work-flow is to provide a consistent methodology to systematically integrate both large-scale geologic elements and small-scale rock petrology with the physical rock properties for low-permeability sandstone reservoirs. To that end, our work-flow integrates multiple data evaluation techniques and multiple data scales using a core-based rock typing approach that is designed to capture rock properties characteristic of tight gas sands.

Fundamental to this process model are identification and comparison of three different rock types — *depositional*, *petrographic*, and *hydraulic*. These rock types are defined as:

- *Depositional* — These are rock types that are derived from *core-based descriptions* of genetic units which are defined as collections of rocks grouped according to similarities in composition, texture, sedimentary structure, and stratigraphic sequence as influenced by the depositional environment. These rock types represent original large-scale rock properties present at deposition.
- *Petrographic* — These are rock types which are also described within the context of the geological framework, but the rock type criteria are based on pore-scale, microscopic imaging of the *current* pore structure — as well as the rock texture and composition, clay mineralogy, and diagenesis.
- *Hydraulic* — These are rock types that are also defined at the pore scale, but in this case we define "hydraulic" rock types as those that quantify the physical flow and storage properties of the rock relative to the native fluid(s) — as controlled by the dimensions, geometry, and distribution of the current pore and pore throat structure.

Each rock type represents different physical and chemical processes affecting rock properties during the depositional and paragenetic cycles. Since most tight gas sands have been subjected to post-depositional diagenesis, a comparison of all three rock types will allow us to assess the impact of diagenesis on rock properties. If diagenesis is minor, the depositional environment (and depositional rock types) as well as the expected rock properties derived from those depositional conditions will be good predictors of rock quality. However, if the reservoir rock has been subjected to significant diagenesis, the original rock properties present at deposition will be quite different than the current properties. More specifically, use of the depositional environment and the associated rock types (in isolation) to guide field development activities may result in ineffective exploitation.

Introduction

Unconventional natural gas resources — tight gas sands, naturally-fractured gas shales, and coalbed methane reservoirs — comprise a significant percentage of the North American natural gas resource base and these systems represent an important source for future reserve growth and production. Similar to conventional hydrocarbon systems, unconventional gas reservoirs are characterized by complex geological and petrophysical systems as well as heterogeneities — at all scales. However, unlike conventional reservoirs, unconventional gas reservoirs typically exhibit gas storage and flow characteristics which are uniquely tied to geology — deposition and diagenetic processes. As a result, effective resource exploitation requires a comprehensive reservoir description and characterization program to quantify gas-in-place and to identify those reservoir properties which control production. Although many unconventional natural gas resources are characterized by low permeabilities, this paper addresses only low-permeability sandstone reservoirs, *i.e.*, tight gas sands.

The oil and gas industry has long recognized the importance of pore structure (*i.e.*, pore and pore throat dimensions, geometry, size, distribution, *etc.*) on fluid flow and storage properties in all types of porous media. Understanding the pore structure and

properties is probably even more critical in tight gas sands since diagenesis often modifies the original pore structure and reduces the average pore throat diameter, typically causing an increase in both tortuosity and the number of isolated and/or disconnected pores. Some forms of diagenesis may actually *increase* porosity by creating secondary or micro-porosity. Regardless of the type of diagenesis, all tight gas sands retain some underlying traits of the depositional system even though the original rock properties may have been (significantly) altered. However, well productivity cannot be predicted accurately based *solely* on the rock properties *expected* for those specific depositional environments and conditions.

Because of the importance of understanding pore-scale rock properties, we are proposing a *rock typing work-flow process developed specifically for tight gas sands*. The concept of rock typing is not new to the petroleum industry. In fact, the petroleum literature is replete with papers describing rock typing techniques for conventional reservoirs. Unfortunately, there is no truly consistent rock type definition — especially for tight gas sands — although there are often similar evaluation techniques and data sources used to identify the rock types. The most widely quoted definition is often attributed to Gunter, *et al.* [1997a and 1997b], but we note that this definition was first given by Archie [1950] who defined a "rock type" as:

...units of rock deposited under similar conditions which experienced similar diagenetic processes resulting in a unique porosity-permeability relationship, capillary pressure profile and water saturation for a given height above free water in a reservoir. (Archie [1950])

Archie's definition implicitly suggests inclusion of depositional system properties, as well as any diagenetic effects in the identification of rock types. This definition also indicates that rocks should be grouped according to physical properties controlling fluid storage, flow, and distribution. We should also note that Archie's reference to "height above free water" in a reservoir may not be applicable to "basin-centered gas systems" [Masters, 1979] which is defined as

... a basin-centered gas system ...is an abnormally-pressured, gas-saturated accumulation in a low permeability reservoir lacking a down-dip water contact. ([Law 2000])

Many basin-centered gas reservoir systems can also be classified as tight gas sands — however; the characterization of basin-centered gas systems typically requires multiphase rock fluid properties (*e.g.*, gas-water capillary pressure, gas-water relative permeability, *etc.*), as well as the role of shale (Is the reservoir dominantly shale? How do the sand/shale sequences interact? *etc.*). Although basin-centered gas reservoir systems are not specifically addressed in this paper, our proposed rock typing approach is applicable to basin-centered gas systems (with extensions, some of which are noted above).

In **Tables 1** and **2** we summarize: rock type definitions, data sources, and evaluation methodologies for selected reservoir description and characterization studies of sandstone and carbonate lithologies (respectively). Inspection of the compiled references shows that most of the technical literature addressing rock typing studies does include some or most of the aspects suggested by Archie's definition. We also observed the following rock types common to several studies:

- *Lithofacies* are defined by Porras, *et al.* [1999] and Perez, *et al.* [2003] as "mappable stratigraphic units, laterally distinguishable from the adjacent intervals based upon lithologic characteristics such as mineralogical, petrographical, and paleontological signatures that are related with the appearance, texture, or composition of the rock." Similar rock types have also been defined as geological facies or simply facies. This definition has been applied to studies of both carbonate and sandstone reservoirs. Both lithofacies and geological facies are identified from either log-based analyses or core-based descriptions and incorporate large-scale elements within the geologic framework.
- *Petrofacies* are defined by Porras, *et al.* [1999] as "intervals of rock with a similar average pore throat radius, thus having similar fluid flow characteristics." Other similar definitions have been referred to as petrophysical rock types, reservoir rock types, and static rock types. Common to all of these rock type definitions is an attempt to correlate the pore structure (*i.e.*, pore and pore throat dimensions, geometry, size, distribution, *etc.*) to physical rock properties such as effective porosity and absolute permeability. Pore system characteristics are typically identified using mercury-injection capillary pressure measurements.
- *Electrofacies* are again defined by Perez, *et al.* [2003] as "a similar set of log responses that characterizes a specific rock type and allows it to be distinguished from other. Electrofacies are obviously influenced by geology and can often be assigned to one or another lithofacies, even though the correspondence is not universal." The electrofacies rock type is similar to the lithofacies in that it is attempting to identify and group rocks based on large-scale geologic features as manifested by the log responses. Based on our literature search, use of the electrofacies rock types appear to be confined to just carbonate reservoirs.

Although all rock typing approaches evaluated from the petroleum literature (and summarized in **Tables 1** and **2**) use similar data sources and evaluation methodologies, none of these studies proposes a comprehensive methodology that is developed specifically to capture rock properties characteristic of tight gas sands. Therefore, the overall objective of this paper is to propose a work-flow process that provides a systematic rock typing process to integrate both large-scale geologic elements and small-scale rock petrology with the physical rock properties in low-permeability sandstone reservoirs. Essential components of our process model are identification, specification, and comparison of three rock types (*i.e.*, the *depositional, petrographic, and hydraulic* rock types).

Table 1 — Summary of Selected Rock Typing Studies and Definitions for Sandstone Reservoirs

Reference	Formation/ Location	Rock Type Definitions	Data Sources / Evaluation Methodologies
Davies, et al. [1991]	Travis Peak sands, East Texas Salt Basin	No specific definitions	<ul style="list-style-type: none"> Depositional environments, sand body geometry, dimensions from core descriptions Texture, composition, lithology from microscopic imaging No quantitative porosity-permeability ranges; provided qualitative indicators
Porras, et al. [1999]	Santa Barbara and Pirital Field sands, Eastern Venezuela Basin	Lithofacies, petrofacies	<ul style="list-style-type: none"> Physical core descriptions of both large-scale & small-scale features; microscopic imaging of texture, composition, lithology, diagenesis Core-based measurement of porosity, permeability; dominant pore throat diameter from mercury-injection capillary pressure data
Davies, et al. [1999]	Wilmington Field Pliocene-Age sands	No specific definitions	<ul style="list-style-type: none"> Depositional environments, sand body geometry, dimensions from core descriptions Texture, composition, lithology from microscopic imaging No quantitative porosity-permeability ranges; provided qualitative indicators
Boada, et al. [2001]	Santa Rosa Field, Eastern Venezuela Basin	Lithofacies, petrofacies	<ul style="list-style-type: none"> Physical core descriptions of both large-scale & small-scale features; microscopic imaging of texture, composition, lithology, diagenesis Core-based measurement of porosity, permeability; dominant pore throat diameter from mercury-injection capillary pressure data
Leal, et al. [2001]	Block IX sands, Lake Maracaibo Basin, Venezuela	Lithofacies, petrofacies	<ul style="list-style-type: none"> Physical core descriptions of both large-scale & small-scale features; microscopic imaging of texture, composition, lithology, diagenesis Core-based measurement of porosity, permeability; dominant pore throat diameter from mercury-injection capillary pressure data
Madariage, et al. [2001]	Sandstone/ C4 & C5 sands, Lagunillas Field, Lake Maracaibo Basin, Venezuela	Lithofacies, petrofacies	<ul style="list-style-type: none"> Physical core descriptions of both large-scale & small-scale features; microscopic imaging of texture, composition, lithology, diagenesis Core-based measurement of porosity, permeability, electrical properties; dominant pore throat diameter from mercury-injection capillary pressure data
Porras, et al. [2001]	Tertiary & Cretaceous sands, Santa Barbara Field, Eastern Venezuela Basin	No specific definitions	<ul style="list-style-type: none"> Physical core descriptions of both large-scale & small-scale features; microscopic imaging of texture, composition, lithology, diagenesis Core-based measurement of porosity, permeability; dominant pore throat diameter from mercury-injection capillary pressure data
Soto, et al. [2001]	K1 sands, Suria & Reforma- Libertad Fields, Apiay-Ariari Basin, Columbia	No specific definitions	<ul style="list-style-type: none"> Core-based measurement of porosity, permeability; dominant pore throat diameter from mercury-injection capillary pressure data Used fuzzy logic to predict rock types in uncored wells
Marquez, et al. [2001]	LL-04 sands, Tia Juana Field, Lake Maracaibo Basin, Venezuela	Lithofacies, petrofacies	<ul style="list-style-type: none"> Identification of stratigraphic units and lithofacies from log analysis Physical core descriptions of small-scale features; microscopic imaging of texture, composition, lithology Core-based measurement of porosity, permeability; up scaled permeability using NMR log measurements
Ali-Nandalal & Gunter [2003]	Pliostocene-age sands, Mahogany Field, Columbus Basin, Venezuela	Geological facies, Petrophysical rock types	<ul style="list-style-type: none"> Facies identified using core- and log-based analyses of primary sedimentary structures Core-based measurement of porosity, permeability and electrical properties
Ohen, et al. [2004]	Shushufindi Field sands, Oriente Basin, Ecuador	Geological facies	<ul style="list-style-type: none"> Facies identified using core- and log-based analyses of stratigraphy, structure, depositional environment Core-based measurement of porosity, permeability and water saturation
Acosta, et al. [2005]	El Furrial Field sands, Venezuela	Geological facies, Petrophysical rock types	<ul style="list-style-type: none"> Facies identified using core- and log-based analyses of stratigraphy, structure, depositional environment Core-based measurement of porosity, permeability and water saturation; pore characteristics from mercury-injection capillary pressure data
Guo, et al. [2005]	Napo formation sands, Oriente Basin, Ecuador	Petrophysical rock type	<ul style="list-style-type: none"> Core-based measurement of porosity, permeability and water saturation; pore characteristics from mercury-injection capillary pressure data
Shenawi, et al. [2007]	Formation unknown, location unknown	Geological facies, Petrophysical rock types	<ul style="list-style-type: none"> Facies identified using log-based definitions of shale content, lithology (density log) Core-based measurement of porosity, permeability and water saturation; pore characteristics from mercury-injection capillary pressure data

Table 2 — Summary of Selected Rock Typing Studies and Definitions for Carbonate Reservoirs

Reference	Formation/ Location	Rock Type Definitions	Data Sources / Evaluation Methodologies
Neo, <i>et al.</i> [1998]; Grottsch, <i>et al.</i> [1998]; Marzouk, <i>et al.</i> [1998]; Al-Aruri, <i>et al.</i> [1998]	Lower Cretaceous-age Thamama I, II, II reservoirs, offshore Abu Dhabi	Depositional facies, Lithofacies, Petrophysical rock types	<ul style="list-style-type: none"> Depositional environments, lithologies identified from core-based descriptions and log-based analysis Petrophysical properties including lithology, grain size & distribution from microscopic imaging; porosity, permeability determined from core analysis; pore structure & geometry determined from mercury-injection capillary pressure data
Mathisen, <i>et al.</i> [2001]	Upper & lower Clearfork formations, North Robertson Unit, Gaines Co., TX	Lithofacies, Electrofacies	<ul style="list-style-type: none"> Geological interpretations & log response to identify basic lithofacies Log-based descriptions based on similarity of log responses reflecting differences in mineralogy & lithofacies
Lee, <i>et al.</i> [2002]; Perez, <i>et al.</i> [2003, 2005]	C1a, C1b, C2a, C2b, C3-C5 zones, Northwest Extension carbonate buildup, Salt Creek Field, Kent Co., TX	Lithofacies, Electrofacies	<ul style="list-style-type: none"> Identified lithofacies using core-based descriptions & microscopic imaging Identified electrofacies using log-based descriptions based on similarity of log responses reflecting differences in mineralogy & lithofacies
Aplin, <i>et al.</i> [2002]	Lower Cretaceous-age Thamama Group, onshore U.A.E.	Lithofacies, Reservoir rock type	<ul style="list-style-type: none"> Identified lithofacies using log-based similarities in micro-resistivity curves; calibrated to core-based descriptions Identified reservoir rock types from core-based physical descriptions, microscopic imaging; evaluated porosity, permeability from core measurements; determined pore structure & dimensions from mercury-capillary pressure data
Al-Habshi, <i>et al.</i> [2003]	Upper Zakum Formation, Field "B", onshore Abu Dhabi	Lithofacies	<ul style="list-style-type: none"> Identified lithofacies from geological interpretations, log and core analyses, and paragenetic sequence analysis Determined physical properties from core measurements; identified diagenesis from microscopic imaging; determined pore structure & dimensions from mercury-injection capillary pressure data
Bieravand [2003]	Upper Cenomanian carbonate reservoir	Lithofacies, reservoir rock types	<ul style="list-style-type: none"> Identified lithofacies from geological interpretations and core-based physical descriptions Evaluated permeability & porosity from routine core analysis; quantified pore structure using mercury-injection capillary pressure data
Al-Farisi, <i>et al.</i> [2004]	Offshore Abu Dhabi carbonate	Electrofacies	<ul style="list-style-type: none"> Evaluated rock fabric & texture from core studies; measured permeability & porosity from routine core analysis, measured pore structure from mercury-injection capillary pressure data Up scaled core-based rock types to electrofacies using log response
Meyer, <i>et al.</i> [2004]	K1-K4 intervals, Upper Khuff Formation, offshore Abu Dhabi	Lithofacies, Static rock types	<ul style="list-style-type: none"> Depositional environments, lithologies identified from geological interpretations, core-based descriptions and log-based analysis Identified static rock types based on pore types determined from microscopic imaging and mercury-injection capillary pressure data
Varavur, <i>et al.</i> [2005]	No information	Lithofacies, Petrophysical rock types	<ul style="list-style-type: none"> Identified lithofacies from geological interpretations and core-based physical descriptions; lithofacies defined based on depositional texture, grain-size, sorting, diagenesis Evaluated permeability & porosity from routine core analysis; quantified pore structure using microscopic imaging and mercury-injection capillary pressure data
Rebelle, <i>et al.</i> [2005]	Lower Kharai formation, onshore Abu Dhabi	Lithofacies, Petrophysical rock types	<ul style="list-style-type: none"> Identified lithofacies from geological interpretations and core-based physical descriptions; lithofacies defined based on depositional texture, lithology, diagenesis Evaluated permeability & porosity from routine core analysis; quantified pore structure using mercury-injection capillary pressure data
Frank, <i>et al.</i> [2005]	Shuaiba formation, Al Shaheen Field, offshore Qatar	No definitions	<ul style="list-style-type: none"> Identified rock types using routine core measurements, microscopic imaging, mercury-injection capillary pressure data, NMR characteristics Up scaled rock types using NMR logs
Creusen, <i>et al.</i> [2007]	Natih formation, Oman	Primary rock types, Rock type associations	<ul style="list-style-type: none"> Primary rock types identified on pore scale using microscopic imaging as well as routine porosity & permeability measurements Rock type associations reflect collections of primary rock types, pore types and size distribution

We begin the next section with the definitions of the rock types that we propose for our reservoir description and characterization work-flow process model. We then discuss the desired data types and measurement techniques for identifying each rock type. In this discussion, we include physical and chemical phenomena which affect the sand quality and continuity. Finally, we illustrate application of the work-flow process using a field case example derived from the Bossier tight gas sand play in the East Texas Basin.

Rock Type Definitions for Tight Gas Sands

Although valid for most conventional oil and gas reservoirs, the rock type definition given by Archie [1950] is too general for tight gas sands since the processes resulting in similar rock properties may not be unique, especially when the rocks have been subjected to significant diagenesis. Accordingly, we integrate three rock types — *depositional*, *petrographic*, and *hydraulic* [Newsham and Rushing, 2001; Rushing and Newsham, 2001]. Each rock type represents different physical and chemical processes affecting the rock properties during both depositional and paragenetic cycles. We define the tight gas sand rock types as follows:

- *Depositional* rock types are defined within the context of the large-scale geologic framework and represent those original rock properties present at *deposition*. The *original* rock properties will vary depending on many factors, including the depositional environments, sediment source and depositional flow regimes, sand grain size and distribution, type and volume of clay deposited, etc. Depositional rock types are based principally upon core-derived descriptions of genetic units representing similar depositional energy, environments, and morphology resulting in unique rock texture, sedimentary structure, and stratigraphic sequence. Depositional rock types help us to define the geological architecture and to describe large-scale reservoir compartments. Mapping the distribution of depositional rock types should also define the extent of the reservoir "container," i.e., gas-in-place.
- *Petrographic* rock types are also described in the context of the geological framework established from the depositional rock types, but are based on a pore-scale microscopic imaging (i.e., thin section descriptions, x-ray diffraction analysis, and scanning electron microscopy imaging of the current pore structure [Neasham, 1977a; Davies, 1990; Pittman and Thomas, 1991]). Constituent mineral distribution, composition and habitat influence the petrographic rock type classification, so the description includes rock texture and composition, clay mineralogy, and diagenesis. Both the framework and matrix components have a "cause and effect" relationship on the diagenetic processes — resulting in preservation, loss, or enhancement of rock properties. Although there is some debate in the industry concerning the impact of the timing of hydrocarbon generation and migration into the reservoir relative to deposition (i.e., the paragenetic sequence) on reservoir quality [Bloch, et al., 2002], the petrographic rock type attempts to quantify these effects.
- *Hydraulic* rock types are also quantified on the pore scale but represent the physical rock flow and storage properties as controlled by the pore structure. The hydraulic rock type classification provides a physical measure of the rock flow and storage properties at current conditions — i.e., reflecting the current pore structure as modified by diagenesis. The size, geometry, and distribution of pore throats, as determined by capillary pressure measurements, control the magnitude of porosity and permeability for a given rock. High-pressure mercury-injection capillary pressure measurements may be calibrated to absolute permeability measurements [Swanson, 1981; Thompson, et al., 1987; Pittman, 1992b; Huet et al., 2005] to help develop permeability-porosity relationships. Correct identification of hydraulic rock types should allow us to develop unique permeability-porosity relationships as a function of the dominant pore throat dimensions.

We note that all three rock types should be similar if the rocks have been subjected to little or no diagenesis. For example, we would expect to observe the permeability-porosity relationships for depositional rock types (derived from geologic models of the depositional environments and processes) to be applicable to petrographic and hydraulic rock types as well. However, as diagenetic effects increase in severity and occurrence, the original rock texture and composition, pore geometry, and physical rock properties will be modified. Under these conditions, we would expect to see no or very poor correlations among the permeability-porosity relationships derived for each of the different rock types. Ultimately, we would then rely upon the permeability-porosity functions developed for the hydraulic rock types since they reflect the current rock properties.

Physical and Chemical Processes Controlling Tight Gas Sand Properties

The low permeabilities (and porosities) associated with tight gas sands can be attributed *directly* to a large distribution of small to very small pores and/or a very tortuous system of pore throats connecting those pores. Further, both small pores and tortuous pore throat systems can result from several processes — including initial deposition of fine to very fine grained sediments, the presence of various types of dispersed shales and clays in the pores [Neasham, 1977b], and/or post-depositional diagenesis that alter the original pore structure. [Holland, 1982; Keighin and Sampath, 1982; Walls, 1982b; Dibble, et al., 1983; Pallatt, et al., 1984; Randolph, et al., 1984; and Luffel, et al., 1991] Therefore, successful exploitation of a tight gas sand reservoir requires a basic understanding of the rock pore structure and properties as well as the processes affecting those properties.

Complicating any description and characterization program is the fact that not all low-permeability sandstone reservoirs are alike, so each program should be designed to address a specific reservoir or field. However, there are common physical and chemical processes controlling tight gas sand properties, so identification of these processes can help to create common elements in a particular description and characterization program. In this section, we provide an overview of basic sandstone reservoir properties and their impact on flow and storage capacities. We also discuss various physical and chemical processes and their effect on rock properties. Following Berg [1986], we divide our discussion of rock properties into two categories — *i.e.*, primary and secondary properties. Primary properties reflect the depositional environment — energy, and sediment flow regimes, including an evaluation of sediment composition and texture as well as sedimentary structure and reservoir morphology. Secondary properties represent diagenesis — which is defined as any post-depositional process (either physical or chemical) causing changes in initial rock properties. We should note that diagenesis is very important since it is the principal cause of both low permeability and low porosity in tight gas sands.

Sediment Composition. The composition of sandstone reservoirs is typically divided into three basic components — grains, matrix, and cements. Grains or framework grains refer to the larger, solid components in the rock. These components form the basic small-scale units of sandstone reservoirs. The original grain composition is controlled by the composition of the sediment source (*i.e.*, provenance) as well as the physical and chemical processes under which the sediments are created and transported to the geologic basin. Often referred to as detrital grains, the grain composition of most sandstone reservoirs consists primarily of quartz, feldspars, and rock fragments [Berg, 1986].

Following deposition and burial, the framework grains are often altered by the physical effects of compaction as well as various chemical processes, *i.e.*, diagenesis. We typically refer to the resulting materials as authigenic grains. We should note that knowledge of the original grain composition is important since it governs the type and severity of diagenesis. For example, some minerals are more brittle and may be more susceptible to compaction and/or failure during burial and the associated increase in stresses. Other minerals may be more reactive to natural fluids within the pores and may be altered (sometimes significantly) by adverse chemical reactions.

The matrix — the second common component in a sediment — refers to the finer materials deposited between the larger grains and typically includes both clays and shales. Clays may also be classified as either detrital or authigenic. Detrital clays originate either from the sediment source material during deposition, or may form from biogenic processes shortly after deposition [Wilson, 1982]. Authigenic clays are formed by some type of chemical process, either by precipitation from formation fluids or regeneration of detrital clays. According to Wilson [1982], clay regeneration refers to "processes in which clays develop by alteration of precursor clays." The principal clay minerals observed in sandstone reservoirs are kaolinite, smectite, illite, and chlorite.

Clays can vary widely in the structure or morphology of both the individual and aggregate particles. Regardless of their structure, the presence in the rock pores generally reduces both permeability and primary porosity; however, the magnitude of these reductions depends on clay type, structure and location in the pores. Wilson and Pittman [1977] have identified detrital clay morphologies commonly observed in sandstone reservoirs as laminae, clasts, grain coats, burrow fills and linings, and dispersed flakes. Wilson and Pittman also note that only the last three clay types listed appear to significantly affect rock permeability (*i.e.*, smectite, illite, and chlorite). Similarly, Neasham [1977b] has identified three general types of dispersed authigenic clays and their impact on porosity and permeability. He has observed that discrete (not inter-grown) particles have the smallest adverse impact, while both pore-lining and pore bridging clay morphologies may significantly reduce rock permeability. All of these observations reinforce the importance of a comprehensive pore-scale program to identify clay type, origin, and the factors controlling its occurrence.

The last major component common for many tight gas sands is the grain cement. The term cement typically refers to any mineral that forms during diagenesis and is precipitated after deposition of both grains and matrix components [Berg, 1986]. As the name implies, cement joins minerals together in a competent mass in the rock and fills the pore system, thus reducing both permeability and porosity. The most common cement compositions in tight gas sands are silica and carbonate. Silica is precipitated as overgrowths or layers on quartz grains. Silica overgrowth cements may form soon after deposition but often continue to develop with increased pressure and temperature during burial. Carbonate cements are often precipitated early after deposition and tend to fill pore spaces between framework grains. Authigenic clay minerals may also act as cements by helping to bind rock particles together.

We should note that, although we have listed "shale" as a matrix component, it may also be classified as a principle sand component (*i.e.*, a grain), or it may occur as a cementing material. Similar to clays, the shale structure and morphology as well as the manner in which it is distributed in the sand pores has a direct impact on rock properties. Structural shale occurs as discrete grains commonly originating from rip-up clasts (materials eroded from surrounding shale) and rock fragments that have been altered from diagenesis. Structural shale will adversely impact rock permeability and porosity if it is present in significant quantities. Laminar shale occurs as thin layers and will primarily affect the vertical permeability. Dispersed shale is defined as that material found within the (sand) pores. The origin of dispersed shale can be either as detrital material transported during the depositional process or authigenic minerals resulting from precipitates. Of all shale types, dispersed shales will most adversely affect rock permeability and porosity as it often lines or fills the pores and pore throats.

Sediment Texture. Important textural attributes in sandstone reservoirs include grain size, sorting, packing, shape, and grain orientation. Texture is a key component in our pore-scale description and characterization program since it not only affects initial rock properties present at deposition, but texture can also impact the rate, magnitude, and severity of diagenesis. Grain size and distribution, sorting, shape and packing also govern the type and magnitude of the original porosity present following sediment deposition, but before significant diagenesis has occurred. Generally, clean coarse-grained materials will have larger, better connected pores, while small-grained sands will have smaller and less well connected pores. Depending on the type and morphology, the presence of smaller matrix materials (*i.e.*, clays and shale) in clean coarse-grained sands will tend to reduce both permeability and primary porosity.

Grain size and sorting may also have an indirect impact on diagenesis. Stonecipher, *et al.* [1984] have suggested that slow movement of fluids through a low-permeability sediment promotes cementation from a higher retention of precipitates in the pore spaces, while higher flow rates result in more leaching. Consequently, we would expect shaly, fine-grained sediments (with associated low permeability) to be subjected to a higher degree of cementation than a cleaner, coarse-grained sandstone. Conversely, the original permeability in cleaner coarse-grained sands may actually increase as a result of leaching as regional fluids flow through the system.

Other (minor) sandstone textural traits include grain shape and orientation. Grain shape is usually expressed as sphericity and roundness. Sphericity is defined as a measure of the grain's deviation from a spherical shape, while roundness is a measure of the roundness of the grain edges [Berg, 1986]. As an example, consider a cube-shaped object which has a high degree of sphericity but not much roundness. Both sphericity and roundness appear to be related to grain size. Grain orientation refers to the preferred direction of the grain's long axes. Neither grain shape nor orientation are measured routinely — moreover; the contribution of either property (grain shape or orientation) has not been established to any degree of certainty.

Sedimentary Structure. Evaluation of sedimentary structure is an important element of the depositional rock typing process since the type of sedimentary structure may help in identifying depositional environment. Included in this evaluation is identification of bed geometry, bedding planes and contacts between beds, and bedding plane orientation. Understanding sedimentary structure is also an important component in optimizing field development activities since bed geometry and dimensions may impact both vertical and lateral continuity which would, in turn, dictate field well spacing and the type of wellbore architecture. For example, significant vertical heterogeneity may determine how effectively horizontal wellbores will recover the hydrocarbons.

According to Berg [1986], sedimentary structure can be divided into primary and secondary elements. Primary sedimentary structures can be furthered divided into three quantitative and/or qualitative descriptive terms. First, sand bedding may be qualitatively described as either stratified or cross-stratified which define the bed inclination relative to the larger sand unit. Secondly, bed thickness is defined qualitatively as either thin- or thick-bedded. The final descriptive term provides a qualitative indication of how parallel a bed or layer may be relative to either other adjacent layers or to larger bed structures. Primary sedimentary structures have been identified in a wide variety of depositional environments ranging from eolian to deep marine environments.

Elements of secondary sedimentary structures refer to the presence and magnitude of bed or soft-sediment deformation which happens after deposition, but before lithification [Berg, 1986]. Bed deformation may be caused by physical or biological processes. Physical sand deformation is an artifact of several processes (*e.g.*, including sliding, slumping, *etc.*) that tend to affect the original bedding geometry present at the time of deposition. Deformation may be described as either contorted or sheared bedding. Contorted bedding is characterized by bed folding, while sheared bedding refers to bed movement along planar surfaces. Often called bioturbation, biological sand deformation is caused by burrowing organisms or plant root growth. Burrowing organisms are often characteristic of marine shelf environments. Depending on the cause, bioturbation may also help to identify the depositional environment.

Reservoir Morphology. Reservoir morphology defines the sand-body dimensions, geometry, orientation, heterogeneity, and continuity as developed by depositional and post-depositional processes. Both sand quality and quantity are controlled by primary and secondary depositional environments and processes. Quantification of the morphology helps define the reservoir architecture and compartments, and ultimately, to determine the original reservoir volume or "container." For example, the gas-in-place volumes and producing characteristics for a "blanket" sand will be much different than for a reservoir characterized by "lenticular" sands. Reservoir morphology will also affect the optimum well spacing to for field development.

Depositional environment and post-depositional diagenesis both have a significant bearing on morphology, including reservoir compartmentalization and heterogeneity. Reservoir compartments refer to intervals or sections of the sand deposits that are mostly or completely isolated (*i.e.*, not in pressure communication) from other parts of the reservoir. Compartments may be created by significant changes in the depositional environment or by post-depositional processes (*i.e.*, diagenesis and/or tectonic activity creating sand pinch-outs, no-flow barriers, *etc.*). Reservoir heterogeneities, which are typically manifested by lateral and vertical variability in permeability and porosity within the same sand body, are mostly caused by post-depositional diagenesis. Most diagenetic processes do not cause completely isolated reservoir compartments — but such processes may yield complex and/or poor quality flow paths, which may result in low productivity for a given reservoir system.

Diagenesis. Diagenesis — defined as *any post-depositional process causing changes in the initial rock properties* — is very important since it is the principal cause of both low permeability and low porosity in tight gas sands. Diagenesis may be either a physical or a chemical process, or it might be a combination of several different types of processes. In fact, diagenesis is frequently caused by very complex interactions between the sediment minerals and pore fluids at elevated reservoir pressure and temperature conditions. Initial diagenetic events are linked directly to the prevailing local depositional environment as well as the sediment composition. Subsequent diagenesis is typically more widespread, often crossing multiple facies boundaries as a result of regional fluid migration patterns [Stonecipher and May, 1990].

The primary diagenetic processes commonly observed in tight gas sands are: mechanical and chemical compaction, cementation, mineral dissolution or leaching, and clay genesis. Mechanical compaction is caused by grain rearrangement, ductile and plastic rock deformation, and fracturing/shearing of brittle materials. Mechanical compaction may be mitigated somewhat by abnormally high pore pressures which tend to reduce stresses transferred to the grain materials. Chemical compaction refers to changes in grain size and geometry caused by chemical reactions enhanced by pressure conditions, *i.e.*, pressure solution. Generally, both mechanical and chemical compaction will reduce both absolute permeability and primary porosity. Permeability is reduced when pore throats are partially or completely closed, while porosity is lowered from a reduction in the primary pore volume.

Cementation is a chemical process in which minerals are precipitated from pore fluids and bind with existing grains and rock fragments. The most common cement compositions in tight gas sands are silica and carbonate. Silica is precipitated as overgrowths or layers on quartz grains. Silica overgrowth cements may form soon after deposition but often continue to develop with increased pressure and temperature during burial. Carbonate cements are often precipitated early after deposition and tend to fill pore spaces between framework grains. Authigenic clay minerals may also act as cements by helping to bind rock particles together. Most cements tend to reduce both permeability and porosity. However, the presence of authigenic grain coats and rims retards quartz cementation and the associated reduction in permeability and porosity by blocking potential nucleation sites for quartz overgrowths on detrital quartz grains [Bloch, *et al.*, 2002]. We should note that authigenic grain coats and rims seem to reduce or prevent precipitation of quartz cements only, but do not affect precipitation of carbonate, sulfites, or zeolites cements [Pittman, *et al.*, 1992a].

Another type of chemical diagenesis is mineral dissolution. A common source of quartz dissolution is pressure solution caused by stress concentrations at grain contacts which results in silica dissolution, diffusion, advection of silica for reprecipitation in adjacent pores, and an associated loss in porosity. Pressure solution processes can only occur at higher temperatures. Another type of mineral dissolution is the leaching of certain mineral grains and cements, often resulting in an increase in primary porosity and/or creation of secondary porosity. A common source of secondary porosity creation is dissolution of carbonate cements which are often precipitated early after deposition and tend to fill pore spaces between framework grains.

Clay genesis refers to authigenic clays created or generated after deposition. Common authigenic clays found in tight gas sands include chlorites, mixed-layer smectite/illites, and illites. Authigenic chlorites typically develop under iron-rich conditions and commonly occur as pore lining (or coating) clays. Since these clays often do not completely cover the detrital grain surfaces, quartz overgrowths may develop on many grains, thus reducing the original primary porosity. We should note that chlorite generally has high micro-porosity between individual crystals. Smectite clays have been observed in sandstones that contain significant amounts of volcanic rock fragments. According to Wilson [1982], clay pore linings that originally consisted of smectite will be transformed to mixed-layer smectite/illite as the sands are buried deeper and the temperature increases. Continued burial may result in a complete transformation to authigenic illite clays. Illites may also form from kaolinite. In fact, illite clays develop either through precursor detrital or authigenic clays [Wilson, 1977, 1982]. Illite crystals can occur either as fibrous, sheet-like or plate structures. Illite fibers tend to break easily and accumulate in pore throats, causing a reduction or loss of permeability. Illite sheets and plates may also reduce permeability by blocking pore throats. Similar to chlorites, illite plates may have micro-porosity which could add to the total pore volume.

Both reservoir pressure and temperature affect the type, magnitude and severity of diagenesis. Many diagenetic reaction rates double with each 10 Deg C increase in temperature [Wilson, 1994]. Moreover, increasing temperatures increases the solubility of minerals and causes the pore waters to become saturated, thereby increasing precipitation and formation of cements. As we have discussed previously, the primary impact of increasing reservoir pressure is mechanical compaction which tends to reduce the primary pore volume. However under some conditions, abnormally high pore pressures may also mitigate mechanical compaction by reducing applied stresses on individual grains.

Data Sources and Evaluation Techniques for Rock Typing Tight Gas Sands

In this section, we outline the recommended data types and measurement techniques for describing and characterizing tight gas sands using our rock typing approach — and we propose rock-type-specific programs with the goal of identifying depositional, petrographic, and hydraulic rock types.

Depositional Rock Types. As we have defined previously, depositional rock types are described within the context of the large-scale geologic framework and represent those original rock properties present at deposition and before significant post-depositional diagenesis has occurred. The original rock properties will vary depending on many factors, including the depositional environments, sediment source and depositional flow regimes, sand grain size and distribution, type and volume

of detrital clay and shale deposited, etc. Therefore, the data acquisition and evaluation program is designed to both qualify and quantify those factors. *Depositional rock types are based principally on geologic interpretations and physical descriptions of whole core.*

Identification of depositional rock types begins with a description of the small-scale geological reservoir architecture. These descriptions are usually derived from interpretations of the structural framework and stratigraphy. Within this framework, genetically related rock packages — both reservoir and non-reservoir rock — are identified and described. For this paper, we define *genetic units as collections of rocks grouped according to similarities in composition, texture, sedimentary structure, and stratigraphic sequence as influenced by depositional environment, energy, and morphology*. We may then infer the depositional flow regime as well as the dominant depositional processes controlling sand-body geometry and orientation from this description.

An important aspect of this rock typing step is developing an understanding of the vertical sequencing of the genetic units. Knowledge of the vertical distribution of depositional rock types helps to define the depositional environment which then leads to a description of the reservoir geometry and flow properties. Interpretation of vertical or stratigraphic sequences also provides an understanding of the overall reservoir architecture which will then allow us to use geological concepts and models to predict locations of the deposition rock types with the best production potential.

Key aspects of the sedimentary rock that may be derived from core descriptions include lithology, texture, biogenic features, and identification of sand beds and sedimentary structure. As we describe later in the section petrographic rock typing, rock lithology may include the mineralogy, composition and color, while texture comprises grain size and distribution, grain shape, rock fabric, and evidence of sorting. Identification of biogenic features, including the type, ages, mode of occurrence and trace fossils, provide clues on the depositional processes. A study of the sedimentary structure and beds will describe bed geometry, identify bedding planes and contacts between beds, and quantify bedding plane orientation.

Since depositional rock types are based principally on *core-derived descriptions* of genetic units, comprehensive core acquisition and evaluation programs are critical for describing these rock types. It is worth noting that core data is also necessary for identifying petrographic and hydraulic rock types. We strongly recommend large-diameter, conventional whole core that should ideally be obtained throughout the entire vertical section, including both reservoir and non-reservoir rock. Complete vertical sections are used for interpreting genetic units into a depositional sequence and predicting depositional environment and architecture. Core data will also help to develop an understanding of reservoir geometry, continuity and distribution of rock types and properties. Although sidewall cores and cuttings can be used to evaluate some rock properties, their small scales make it very difficult to identify any large-scale geologic properties accurately. Consequently, we recommend using sidewall cores only to supplement a whole core program, rather than as the primary source of rock material.

Petrographic Rock Types. Petrographic rock types are described on the pore-scale but within the context of the large-scale geologic framework identified from the depositional rock typing evaluation step. *The primary tools used for describing petrographic rock types are microscopic imaging techniques — i.e., thin section descriptions, x-ray diffraction analysis, and scanning electron microscopy imaging.* Included in these evaluations are descriptions of sediment source, rock composition and texture, mineralogy, and clay types. An important component of the petrographic rock typing is an assessment of the types of diagenesis and the potential impact on rock flow and storage capacity. We also recommend supplementing the microscopic image processes with pore geometry and other properties as identified from mercury-injection capillary pressure measurements.

Thin Section Analysis. Thin section studies utilize optical techniques to identify rock texture, composition, and quality (*i.e.*, certain aspects of the pore structure and volume). Thin sections are typically constructed of ultra-thin slices (30 microns thickness) of rock in which the pore volume is impregnated under a vacuum with a low-viscosity blue or red fluorescent epoxy resin. Most minerals will transmit light at a thickness of 30 microns, so we are able to evaluate the pore structure, framework grains, and matrix material from transmitted polarized light microscopy. In some instances, stains may be added to help with identification of specific minerals.

Thin section analyses allow us to assess the rock composition including the type and quantity of framework grains, pore-filling matrix, and cementing materials. Common framework grains (*i.e.*, quartz, feldspars, mica, etc.) can be identified and differentiated based on differences in optical properties. The composition of most common cementing minerals can also be determined providing the cement crystal sizes are greater than about 0.015 mm. Similarly, we *cannot* assess the composition of most clays and shales because of microscope magnification limitations. However, we can usually evaluate the relative quantity and the primary location of clays and shales in the rock pores. We can also quantify the average framework grain size as well as the distribution of grain sizes from thin section analysis.

Thin section analysis also allows us to identify the types of porosity in the rocks including both primary and secondary inter-granular porosity, detrital matrix porosity, micro-porosity, and grain fracture porosity. Inter-granular porosity exists as pore spaces between the rock framework grains. Micro-porosity and secondary porosity, which are often important storage components in many tight gas sands, may also be observed using an epifluorescent material and reflected light microscopy. Fracture porosity, also much smaller than inter-granular porosity, is created from micro-fractures in the rock material.

We should note that thin section analyses provide a two-dimensional view of a three-dimensional system, so we cannot view all of the complexities in the pore structure. Another limitation is that of particle size. The standard thin section sample size is approximately 20 mm, so we cannot view any rock fragments greater than that. Limitations on the magnification capabilities of typical petrographic microscopes control our ability to identify the composition of rock fragments smaller than most clays and shales.

X-Ray Diffraction Analysis. X-ray diffraction (XRD) is more of a qualitative technique that provides information on the average rock composition from a determination of the mineral atomic structure. All materials with a crystalline structure (particularly clays and shales) exhibit a unique x-ray diffraction pattern — so XRD irradiates samples with x-rays and allows us to identify rock composition from the diffracted energy characteristics. X-ray diffraction analysis is frequently used to identify the type of clays present in a rock sample.

There are typically two XRD analyses required for rock samples — bulk and clay-sized particles. Bulk or whole rock x-ray diffraction analysis is conducted on the entire rock sample to identify the relative quantity of all minerals. We should note that bulk XRD analysis is accurate for mineral quantities greater than about 10 percent, but cannot accurately identify mineral volumes much less than that. The most common application of bulk XRD analysis is to identify the relative volumes of the primary framework grains, carbonates, and total clay. We should note that bulk XRD analysis is not recommended for evaluating the presence and quantity of individual clay components. Clay-sized or fine-fraction x-ray diffraction analysis is used to evaluate the fine and very fine-grained portion of the rock sample, and is the recommended technique for identifying the type and quantity of specific clay mineral components. The volume of clays present is determined from a comparison of bulk and clay-size XRD analyses.

Scanning Electron Microscopy. Scanning electron microscopy (SEM) analyses are an excellent tool for evaluating the rock pore and pore-throat system, as well as the degree of connectivity among all pores. SEM can also provide information on mineralogy, clay content, and both pore-filling and pore-lining cements and clays. We may also identify natural fractures, diagenetic features, and fossil content.

Rock samples are analyzed by first coating them with a conductive material and then bombarding them with electrons in a vacuum. Black and white images may be constructed from measurements of secondary electron emissions. The scanning electron microscope can magnify images at various levels up to 100,000 times. Consequently, SEM analysis is routinely used to analyze small grains and crystals, particularly clays and other very small pore filling materials.

Mercury-Injection Capillary Pressure Measurements. Capillary pressure data from mercury injection is an effective technique to quantify pore geometry — particularly the size and distribution of pore bodies and throats [Purcell, 1949; Wardlaw and Taylor, 1976]. Mercury is a near-perfect non-wetting fluid phase, but it will enter the rock pores *only when pressure is applied*. Larger pore spaces are saturated initially, but mercury progressively invades smaller pore spaces as pressure is increased. If a sufficiently high pressure is reached, then the entire connected pore system, including even the smallest pore throats, can be completely saturated. The magnitude of the entry or displacement pressure reflects the largest connected pore throat in the system. In addition, the curvature and rate of increase of the capillary pressure data characterize the size and distribution of the pores. We may also identify bi-modal pore size distributions from the shape of the capillary pressure data.

Hydraulic Rock Types. Similar to the petrographic rock typing step, hydraulic rock types are also quantified on the pore scale but represent the *physical* rock flow and storage properties as controlled by the pore structure. Hydraulic rock type classification provides a measure of the rock flow and storage properties at current conditions, *i.e.*, reflecting the current pore structure as modified by diagenesis. *The primary tools for identifying hydraulic rock types are routine core analysis* which includes measurements of total and effective porosity, absolute permeability, and pore size and distribution from mercury-injection capillary pressure data.

Total and Effective Porosity. Porosity, which is a measure of the rock's storage capacity, is affected not only by the primary depositional processes but also by all subsequent diagenetic processes. Porosity is typically classified into two fundamental types — effective and total [Amyx, Bass and Whiting, 1960]. Effective porosity quantifies only that pore volume that is connected, while total porosity is a measure of all pore volumes, regardless of their connectivity. In conventional sandstone reservoirs with little or no diagenesis, effective porosity is often slightly less than total porosity. However, effective porosity in tight gas sands is typically much lower than the total porosity because of diagenesis. The type and magnitude of diagenesis governs the connectivity of the primary porosity.

Unlike conventional sandstone reservoirs that are characterized mostly by a primary inter-granular porosity system, tight gas sands may exhibit several other types of porosity — including both primary and secondary inter-granular porosity, detrital matrix porosity, micro-porosity, and grain fracture porosity. Inter-granular porosity exists as pore spaces between the rock framework grains — micro-porosity (which is typically associated with clays and shales), is usually much smaller than inter-granular porosity. Unfortunately, we cannot uniquely distinguish among various porosity types or quantify these porosity types directly with physical measurements — we can, however, use microscopic imaging to estimate relative percentages.

There are several laboratory methods to measure effective porosity in tight gas sands. Common to all techniques are measurement of two of the three volumes associated with porosity calculations, *i.e.*, bulk (V_b), matrix or grain (V_m), and pore (V_p) volumes [Amyx, Bass and Whiting, 1960]. Porosity, written in terms of these three volumes, is:

The resaturation or Archimedes method saturates the core with a liquid of known density, and estimates the pore volume (V_p) from the difference between saturated and unsaturated core weights. Bulk volume (V_b) is estimated from the buoyancy of the saturated core when the core is submerged in the same liquid used to saturate the pore spaces. This method is not recommended for tight gas sands since it is often difficult to saturate low-permeability rock completely with a liquid, and incomplete saturation of all pores would cause errors in the porosity measurements [Luffel and Howard, 1988]. Gas expansion methods, which utilize Boyles Law to estimate the pore volume (V_p) and/or the matrix volume (V_m), are the most accurate techniques for estimating effective porosity in tight gas sands. Typically, helium is used as the saturating gas for the gas expansion methods because of its small molecular weight.

Absolute Permeability. According to Amyx, Bass, and Whiting [1960], permeability is defined as "a measure of the rock's ability to transmit fluids." In particular, absolute or specific permeability is the "permeability to one fluid when the rock is completely saturated with that same fluid." Permeability is affected by most pore-scale rock properties, *i.e.*, texture, composition, and diagenesis. Textural components include grain size, sorting, grain angularity and packing. In general, clean coarse-grain materials have larger and better connected pores, while small-grain sands have smaller and less well-connected pores. Clay composition, distribution, and structure in the pore throats may also significantly impact a rock's permeability.

Permeability can be measured with either a steady-state or unsteady-state permeameter. Steady-state measurements are based on the observation that, under steady-state flowing conditions, the pressure gradient is constant and is directly proportional to the fluid velocity. The constant of proportionality is the absolute core permeability (k) as defined by Darcy's Law:

$$\frac{dp}{dx} = -\frac{\mu}{k} v_x \quad \dots \dots \dots \quad (2)$$

For cores with permeabilities less than about 0.1 md, steady-state flow is difficult to achieve over a reasonable test time, especially when liquid is the flowing fluid (recall that pressure drop stabilization is generally considered to be the "steady-state" criterion). As such, gas is routinely used to estimate permeability for low-permeability core samples. However, gas flow in tight gas sands is often affected by several phenomena which may cause deviations from Darcy's law. Failure to account for these non-Darcy effects, principally *gas slippage* and *inertial flow*, may yield significant error in the estimated permeability values.

Gas slippage effects occur when the size of the average rock pore throat radius approaches the size of the mean free path of the gas molecules — thus causing the velocity of individual gas molecules to accelerate or "slip" when contacting rock surfaces [Amyx, Bass and Whiting, 1960]. This phenomenon is especially significant in tight gas sands that are typically characterized by very small pore throats. Klinkenberg [1941] showed the computed permeability to gas is a function of the mean core pressure — and he also observed the gas permeability approaches a limiting value at an infinite mean pressure (*i.e.*, the higher the pressure, the closer the permeability estimate is to the correct value). This limiting permeability value, which is sometimes referred to as the equivalent liquid permeability or the Klinkenberg-corrected permeability, is estimated from the straight-line intercept (extrapolation) on a plot of measured permeability against reciprocal mean pressure.

In equation form, the "Klinkenberg" line is defined by:

$$k = k_\infty(1 + b/\bar{p}) \quad \dots \dots \dots \quad (3)$$

where k_∞ is the Klinkenberg-corrected permeability, and b is the gas slippage factor.

Inertial effects usually occur at high flow rates and are a result of convective flow as fluid particles move through tortuous rock pore throats of varying sizes. Unlike steady-state Darcy flow, inertial effects are manifested by an increase in the pressure change without a corresponding or proportionate increase in fluid velocity. This additional pressure change is associated with dissipation of inertial energy as fluid particles accelerate through smaller pore throats and decelerate through larger areas. Furthermore, the fluid acceleration creates secondary flow patterns and an irreversible conversion of kinetic energy to heat through viscous shear [Katz, *et al.*, 1959]. Early experimental research [Fancher, *et al.*, 1933; Johnson and Taliaferro, 1938; Green and Duwez, 1951] has documented inertial effects from gas flow in porous media and showed how the equation attributed to Forchheimer [1901]:

$$\frac{dp}{dx} = -\frac{\mu}{k} v_x + \beta \rho v_x^2 \quad \dots \dots \dots \quad (4)$$

is suitable for modeling these effects. Equation 4 indicates that, in single-phase fluid flow through a porous medium, both viscous and inertial forces counteract the externally applied force [Geertsma, 1974]. Note that inertial forces, as represented by the second term on the right side of Eq. 4 and quantified by the inertial resistance coefficient (β) become more important as the fluid velocity increases. Conversely, viscous flow, which is modeled by the first term on the right side of Eq. 4, dominates when flow rates are low. Comparing Eqs. 2 and 4, we note that the Darcy equation (Eq. 2) is a special case of the Forchheimer equation (Eq. 4) when the inertial effects are negligible (*i.e.*, when $\beta \approx 0$).

Unfortunately, there may be significant errors in permeability when the steady-state techniques are used if the steady-state flow condition is not achieved. Specifically, the long test times sometimes required to achieve steady-state flow preclude the use of steady-state techniques for some tight gas sands. Consequently, most commercial laboratories use unsteady-state techniques to estimate permeabilities in tight gas sands. The advent of efficient personal computers, high-speed data acquisition systems, and accurate pressure transducers has contributed to significant improvements in computer-controlled equipment that allows rapid and simultaneous measurement of Klinkenberg-corrected permeability, gas slippage factor, and the inertial resistance coefficient in tight gas sands [Jones, 1972; Walls, 1982a; Keelan, 1986; Jones, 1994]. However, care must be taken in the case of unsteady-state permeability estimation, particularly with the type of gas used in the unsteady-state permeability measurement process [Rushing, *et al.*, 2004].

Field Example: Bossier Tight Gas Sand Play, East Texas Basin

In this section, we illustrate our rock typing approach with an example from the Bossier tight gas sand play in the East Texas Basin. Located in the east-central part of Texas, this play has been one of the most active unconventional natural gas plays (*i.e.*, tight gas sands) in North America over the last ten years. Much of the previous and current Bossier sand development activity has been concentrated in several fields positioned along the western shelf margin of the East Texas Basin. One of these fields has been the subject of extensive geological and petrophysical studies over the last few years, so a vast data base is available to illustrate our rock typing work-flow process. A comprehensive Bossier sand description program (including more than 1,000 ft of whole core obtained from three wells in the subject field) provide the base data for this study. In order to evaluate the sedimentary structure and depositional environment, the entire Bossier section — including both reservoir and non-reservoir rock, has been cored. We present the geological and petrophysical interpretations from one of the cored wells, the ETX Well No. 1.

Regional Geology and Depositional Environment, Bossier Sands. The Jurassic-age Bossier sands were deposited in the East Texas Basin which is described as a deep, elongated trough structure with shelf-slope systems on the flanks. Several major tectonic features — the Sabine Uplift to the east, the Mexia-Talco Fault System to the north and west, and the Angelina-Caldwell Flexure to the south — define the physical basin boundaries [Montgomery, 2000]. The basin, which is recognized as one of three major salt provinces in the US, is also characterized by several major salt features within its interior. Geologic models suggest a relationship between generation of the major fault systems, salt deformation and migration, basin subsidence, and sediment deposition during middle to late Mesozoic. Significant salt structures also appear to control distribution of sediments within the basin interior [Montgomery, 2000].

A typical East Texas Basin stratigraphic column is presented in **Fig. 1** and shows the Bossier sands are part of the Upper Jurassic Cotton Valley Group. The Bossier interval is a thick, lithologically complex black to gray-black shale inter-bedded with fine-grained argillaceous sandstone. The overlying Cotton Valley Sandstones are also comprised of inter-bedded shale and quartz-rich sandstone layers. The Cotton Valley Group is underlain regionally by the Upper Jurassic Louark Group, which includes other hydrocarbon-bearing formations such as the Smackover carbonates and Haynesville/Cotton Valley Limestones. Overlying the Cotton Valley Group is the regionally productive Lower Cretaceous Travis Peak formation.

A schematic diagram of the generalized regional dip-section is presented in **Fig. 2** and shows Bossier sand deposition as cycles of sand progradation into the basin and onto organic-rich mud, succeeded by marine transgression. Much of the complete Bossier interval down-dip appears to be time equivalent to the Cotton Valley Sandstones up-dip and represents pro-delta/delta-front material related to Cotton Valley deltaic systems. The Bossier sands probably originate from the north and west and were transported down-slope by several processes including slumping, debris flow, and turbidity currents. Significant Bossier sand thickness is located in topographic lows created by a combination of faulting, subsidence, and salt movement within the basin. As a comment, most of the productive fields in the Bossier sand have been discovered in these topographic lows.

Regional Overview of the Bossier Shales. The Bossier shale is not only the basal formation for much of the Cotton Valley Group, but it is also inter-bedded with isolated sands throughout most of eastern Texas and northwestern Louisiana. These shales are typically black, organic-rich, calcareous, fossiliferous, marine deposits which are the primary source rock for much of the entire Upper Jurassic and Lower Cretaceous vertical section. Thinner shale intervals in the western part of the basin thicken to the east correlative to general depositional patterns in the East Texas Basin. Source rock quality is generally poorer in the western and northwestern parts of the basin, but improves significantly easterly towards the basin center. From west to east, the near-shore sand and low-stand fan deposits are usually completely encased in the marine Bossier shale.

Local Bossier Sand Geology. The Bossier sands in subject field are comprised of a series of stacked sand-shale packages, illustrated by the type log shown in **Fig. 3**. In chronological order of deposition, these sand packages are the Bonner/York, Shelley, and Moore sands. Stratigraphic sequences observed from several whole cores indicate the sands were deposited as a prograding sediment wedge complex during a low stand onto organic shelf mud deposited during a high-stand. At the top of the sand packages, transgressive lag deposits have been observed indicating the onset of a marine transgression during which very little sand was preserved above wave base. Bossier sands are capped by restricted to open shelf muds deposited during another high-stand.

Typical Bossier sand-body geometry in the subject field is elongated with the long axis typically oriented parallel to the depositional dip, so lateral continuity along depositional strike is often limited. The sand-body thickness varies from tens to

several hundred feet. The combination of low depositional relief and limited lateral sand continuity minimizes the hydrocarbon column height potential within each sand body. In addition, the elongated geometry of the isolated sand bodies combined with low permeability and sometimes significant heterogeneity limit the volume of recoverable gas from a single well, thus requiring well spacing ranging from 40 to 20 acres per well.

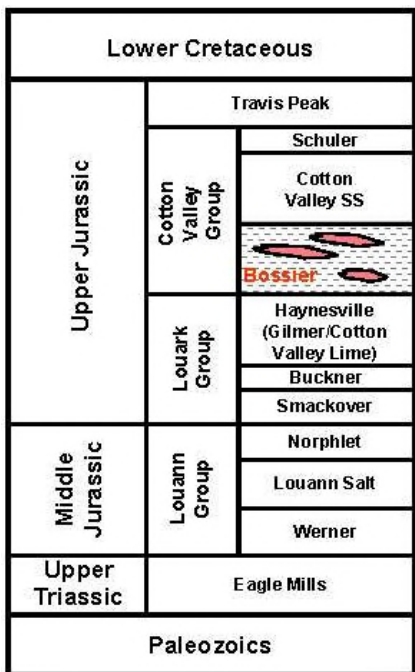


Fig. 1 — Stratigraphic column for Cretaceous and Jurassic section, East Texas Basin.

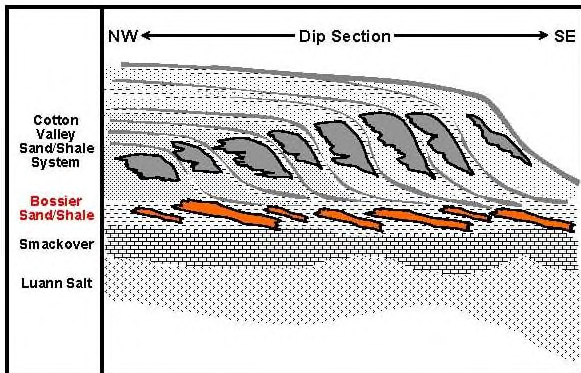


Fig. 2 — Schematic diagram illustrating regional dip-section depositional model for Bossier sands.

Local Geology of Bossier Shales. Bossier shales are prevalent both laterally and vertically in the subject field. Laterally extensive shales appear to act as both seals and hydrocarbon source rock for the sands, while local inter-bedded shales are probably an important hydrocarbon source for the Bossier sands. A study of shale cuttings and core material indicates current total organic carbon ranges from 1 to 5 percent, while the kerogen type is mixed Type II and III. Vitrinite reflectance measurements average 1.25 percent but range from 1.2 to as high as 2.5 percent, indicating the shales are in the "gas window" for hydrocarbon generation.

Gas generation from the shales is the most likely source of the abnormally high pressures measured in the Bossier section in the field. Laboratory data suggests hydrocarbons have been generated not only from kerogen cracking in the shales but also from cracking of liquid hydrocarbons trapped in the sands during initial hydrocarbon migration. This cracking phenomenon [Hunt, 1990] has been postulated on the basis of pyrobitumen observed in core thin sections. Computed carbon isotope separations ($\delta^{13}\text{C}$) for the Bossier gas range from -30 to -40 ppt, which is consistent with gases of thermal origin. The composition of produced gases is primarily methane, but we also observe some ethane and small quantities of propane which is also indicative of thermal (rather than biogenic) origin.

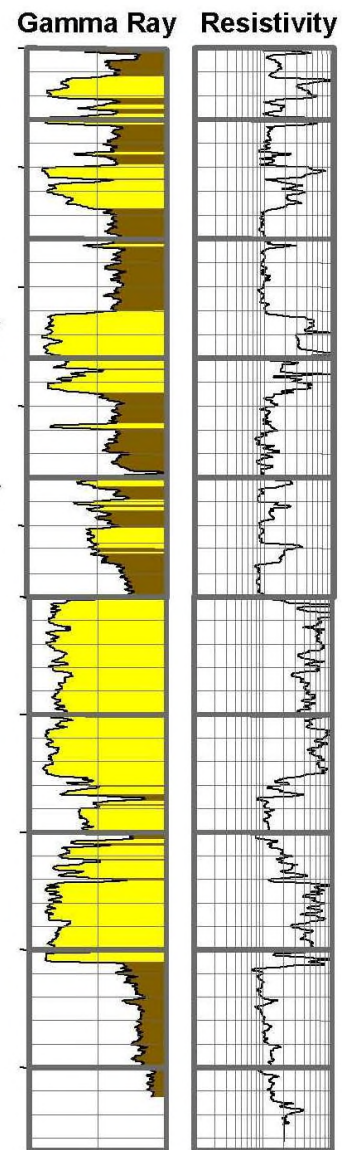


Fig. 3 — Type log for the Bossier sand-shale section, Freestone County, TX., East Texas Basin.

Depositional Rock Types, ETX Well No. 1. The ETX Well No. 1 was drilled in early 2001. As part of the drilling program, we also obtained almost 260 ft of 3 ½-inch diameter whole core over the entire Bossier interval. In this particular part of the field, the Upper Bossier sands (Moore and Shelly) were absent, so only the Lower Bossier sands (Bonner and York) were cored. We cored the entire Lower Bossier interval including both "reservoir" and "non-reservoir" intervals. The core was obtained using an oil-based drilling mud in order to mitigate damage to in-situ rock properties and to improve our connate water saturation estimates from the core analysis. Following acquisition of the core, we conducted a detailed geological evaluation and core description. Much of the geologic interpretation was made using the existing regional Bossier sand geological model as well as the other core samples obtained in the field.

Based on the geological interpretations, we have identified eleven different *depositional* rock types (DRT). The geological interpretations were made in the context of the existing regional Bossier sand depositional models and with supporting data from other cored wells in the field. Summaries of the core descriptions, rock petrology, depositional environments and rock types are shown in **Figs. 4-8** for cores 1-5, respectively. The eleven depositional rock types (DRT) are as follows:

- Distal delta front (DRT 1).
- Transgressive delta front (DRT 2).
- Slumped delta front (DRT 3).
- Distal delta front with slumped medial delta front deposits (DRT 4).
- Delta front to distributary mouth bar (DRT 5).
- Distributary mouth bar to delta front with slumps (DRT 6).
- Proximal delta front to distributary mouth bar with slumps (DRT 7).
- Distributary mouth bar (DRT 8).
- Slumped delta front to distributary mouth bar with thin open shelf (DRT 9).
- Transgressive open shelf (DRT 10).
- Deep open shelf (DRT 11).

Rock textures ranged from siltstones, silty sandstones, and fine-grained to very-fine grained silty sandstones and sandstones. We also see shales and silty shales inter-bedded with the sand and silt. Most, if not all, of the sandstone is comprised of fine to very fine grains suggesting low original porosity. We also observe some dolomitic rock fragments as well as thin carbonate laminations inter-bedded with shale, siltstone, and sandstone. There is some physical evidence of porosity ranging from mostly inter-particle to some secondary dissolution pore. However, many of the intervals have little or no visible porosity.

Sedimentary structures include thin-bedded laminations of shale, silty shale, siltstone and sandstone. Laminations are typically characterized by beds of planar to undulose laminations. In some intervals, we observe non-planar laminations with bedding planes inclined as much as 30 degrees or beds disturbed by burrowing. Ripple structures ranged from climbing ripples, starved ripples, and oscillation ripples. In some cases, we observed possible bi-directional flow with flow-angle cross-bedding. There is also significant evidence of bed disturbance from soft-sediment deformation including contorted/convolution beds, fluidization, fluid escape structures, and small-scale faults possibly caused by localized bed slumping.

Petrographic Rock Types, ETX Well No. 1. Petrographic rock types (PRT) have been identified based on similar constituent mineral distribution, composition, and habitat using thin section descriptions, x-ray diffraction analysis, and scanning electron microscopy imaging. Thin sections were prepared by impregnating the rock with blue epoxy to highlight pore space, grinding to a thickness of 30 microns and staining with Alizarin red to help distinguish calcite. Scanning electron microscopy was used primarily to document the effects of mineral diagenesis on the pore structure and to identify clay types and structure within the pore structure. X-ray diffraction analysis was used to provide semi-quantitative data on the bulk and clay-fraction mineralogy. We also used mercury injection capillary pressure measurements to estimate the pore size distributions in the various rock samples.

We identified four primary *petrographic* rock types based on the pore-scale petrographic study. Most of the analyzed samples are upper very fine- to lower fine-grained sandstones that vary in terms of the inter-granular clay content and diagenetic cements. Some of the samples are more clay-rich, ranging from argillaceous, silty sandstone to silty claystone. The petrographic rock types and the representative sample depths are summarized in **Table 3** with the rock descriptions and the median pore throat dimension determined from mercury-injection capillary pressure data.

Rock Texture. Petrographic rock type 4 (PRT 4) samples have the most argillaceous character, and most seem to have been heavily burrowed, resulting in a more heterogeneous fabric. The samples also have different grain textures and framework grain size. Specifically, the amount of sand-size grains decreases from PRT 4a (13,034 ft), where fine- to very fine-grained sand is abundant, to PRT 4b (13,306 ft) where sand grains are rare. Conversely, the amount of argillaceous siltstone and claystone increases. Burrowing tends to create mixtures of the different rock types by disrupting the original laminated fabric.

Samples PRT 4a and PRT 4c also contain large (1-3 mm) randomly oriented shell fragments. The remaining samples have a grain supported fabric consisting of very fine to occasionally fine sandstones. Samples PRT 1b (13,138 ft) and PRT 1d (13,221.1 ft) are the coarsest and are, on average, lower fine-grained (0.14 mm). Samples PRT 3d (13,171 ft) and PRT 3g (13,203 ft) appear to be the finest grained. The very fine sandstones contain silt-size grains and maximum grain size is

commonly in the upper fine-grained sand range (0.16 – 0.22 mm). Grains up to lower medium sand (0.30 mm) are scattered in the coarser sandstones. The cleaner sandstones are well to well near moderately sorted; however, for the sandstones containing inter-granular detrital clay, the sorting decreases to poor near moderate.

Table 3 — Summary of Petrographic Rock Types and Their Representative Sample Depths

Petrographic Rock Type (PRT) No.	Petrographic Rock Type (PRT) Description	Sample Depth (ft)	Median Pore Diameter (microns)
1a	Fine- to very fine-grained clean sandstone; extensive quartz cement; minor ankerite; variable argillaceous rock fragments (laminated)	13,112	0.1468
1b	Fine- to very fine-grained clean sandstone; extensive quartz cement; minor ankerite; variable argillaceous rock fragments (laminated); minor leached grain pores	13,138	0.2120
1c	Fine- to very fine-grained clean sandstone; extensive quartz cement; minor ankerite; variable argillaceous rock fragments (laminated); minor leached grain pores	13,209	0.2380
1d	Fine- to very fine-grained clean sandstone; extensive quartz cement; minor ankerite; variable argillaceous rock fragments (laminated); minor leached grain pores	13,221	0.2002
2a	Fine- to very fine-grained sandstone, quartz cement, late state calcite cement	13,095	0.0694
2b	Fine- to very fine-grained sandstone, quartz cement, late state calcite cement	13,121	0.0305
3a	Fine- to very fine-grained sandstone; argillaceous; dark brown clay (homogeneous)	13,131	0.0747
3b	Fine- to very fine-grained sandstone; argillaceous; mixed brown and dark brown clay (homogeneous)	13,148	0.0515
3c	Fine- to very fine-grained sandstone; argillaceous; mixed brown and dark brown clay (homogeneous)	13,168	0.1230
3d	Fine- to very fine-grained sandstone; argillaceous; mixed brown and dark brown clay (homogeneous)	13,171	0.0846
3e	Fine- to very fine-grained sandstone; argillaceous; mixed brown and dark brown clay; gradational change in clay	13,176	0.0462
3f	Fine- to very fine-grained sandstone; argillaceous; brown clay (detrital in appearance)	13,199	0.0129
3g	Fine- to very fine-grained sandstone; argillaceous; brown clay (detrital in appearance)	13,203	0.0557
4a	Argillaceous silty, fine- to very fine-grained sandstone; silty claystone laminations, burrowed; large shell fragments	13,034	0.0086
4b	Argillaceous, very sandy, silty claystone; single lamination of calcite cemented sandstone; small shell fragment	13,036	0.0084
4c	Argillaceous siltstone to silty claystone; laminated; burrows, large shell fragment	13,276	0.0080

A few of the samples have indications of bedding or lamination structures as observed from the thin sections, including slight textural grading (**Figs. 9a** and **9b**), faint laminae created by concentrations of argillaceous rock fragments (**Figs. 9c**, **9d**, and **9b**) and more commonly wispy (anastomosing) laminae largely comprised of elongate organic particles (**Figs. 9a** and **9e**). Several of the samples also appear to contain burrows (**Figs. 9f** and **9e**), suggesting the introduction of clay in some of the argillaceous sandstones may be at least partially controlled by biogenic activity. All samples have been magnified 125 times.

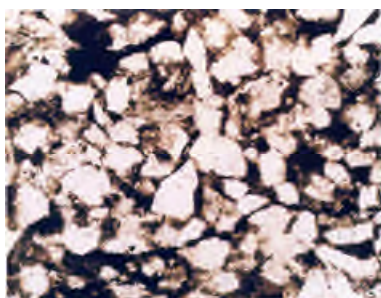


Fig. 9a — Sample PRT 3b (13,148 ft)

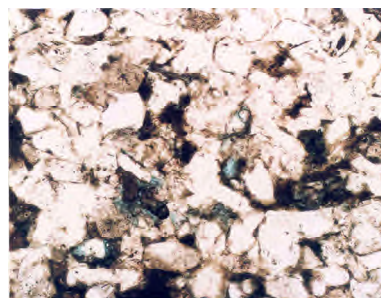


Fig. 9b — Sample PRT 1c (13,209 ft)

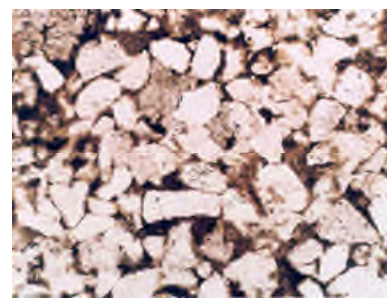


Fig. 9c — Sample PRT 2a (13,095 ft)

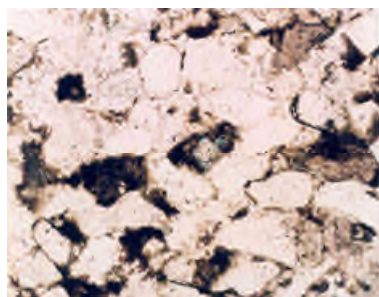


Fig. 9d — Sample PRT 1b (13,138 ft)

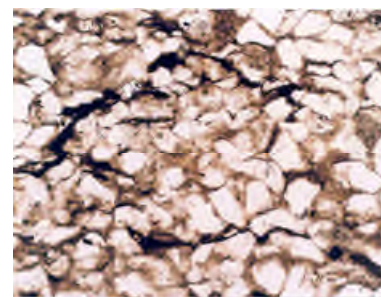


Fig. 9e — Sample PRT 3f (13,199 ft)



Fig. 9f — Sample PRT 3e (13,176 ft)

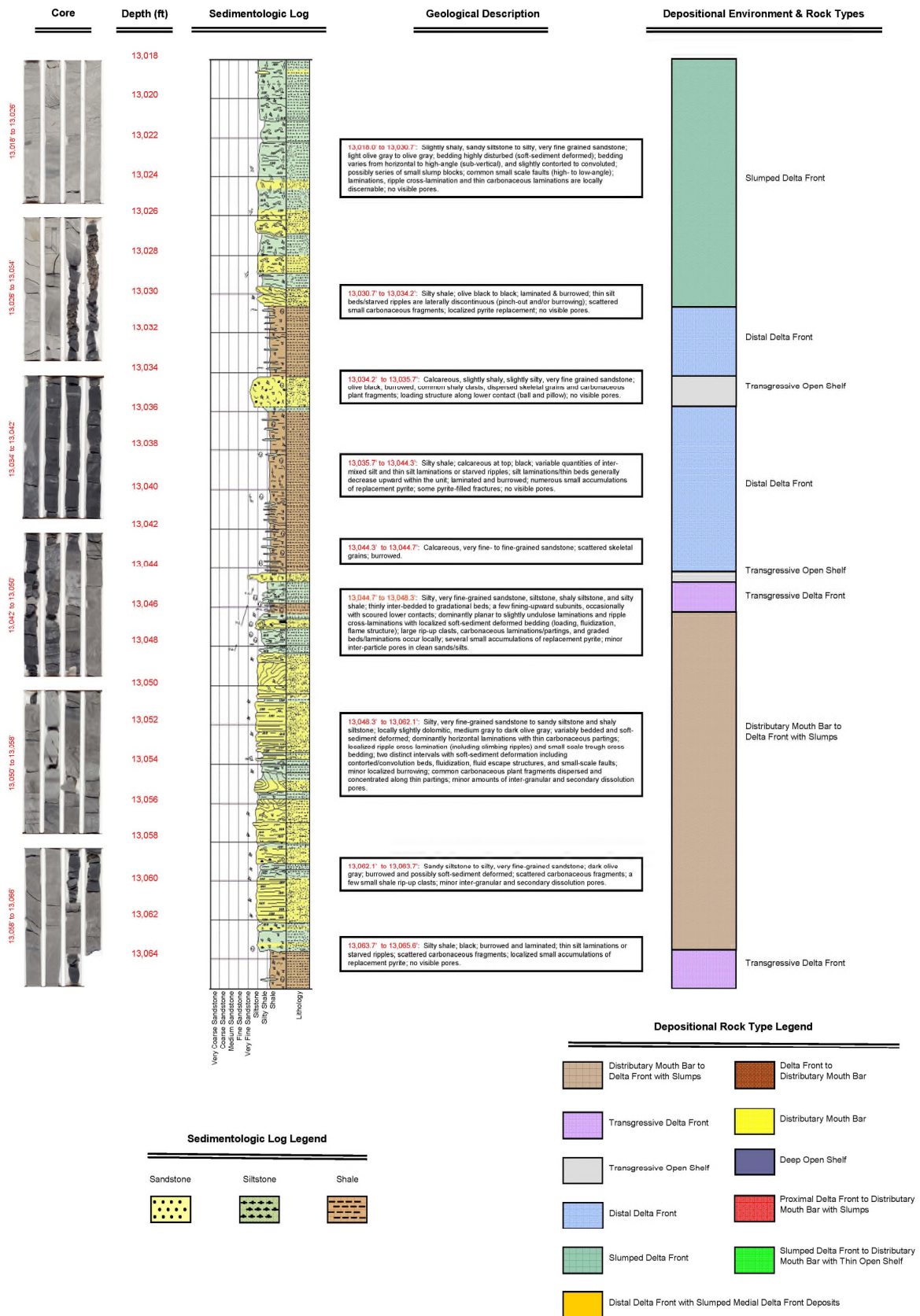


Fig. 4 — Core description, sedimentological log, and depositional environments and rock types for core No. 1 in the interval 13,018.0 ft to 13,065.6 ft, Lower Bonner and Upper York sands, ETX Well No. 1.

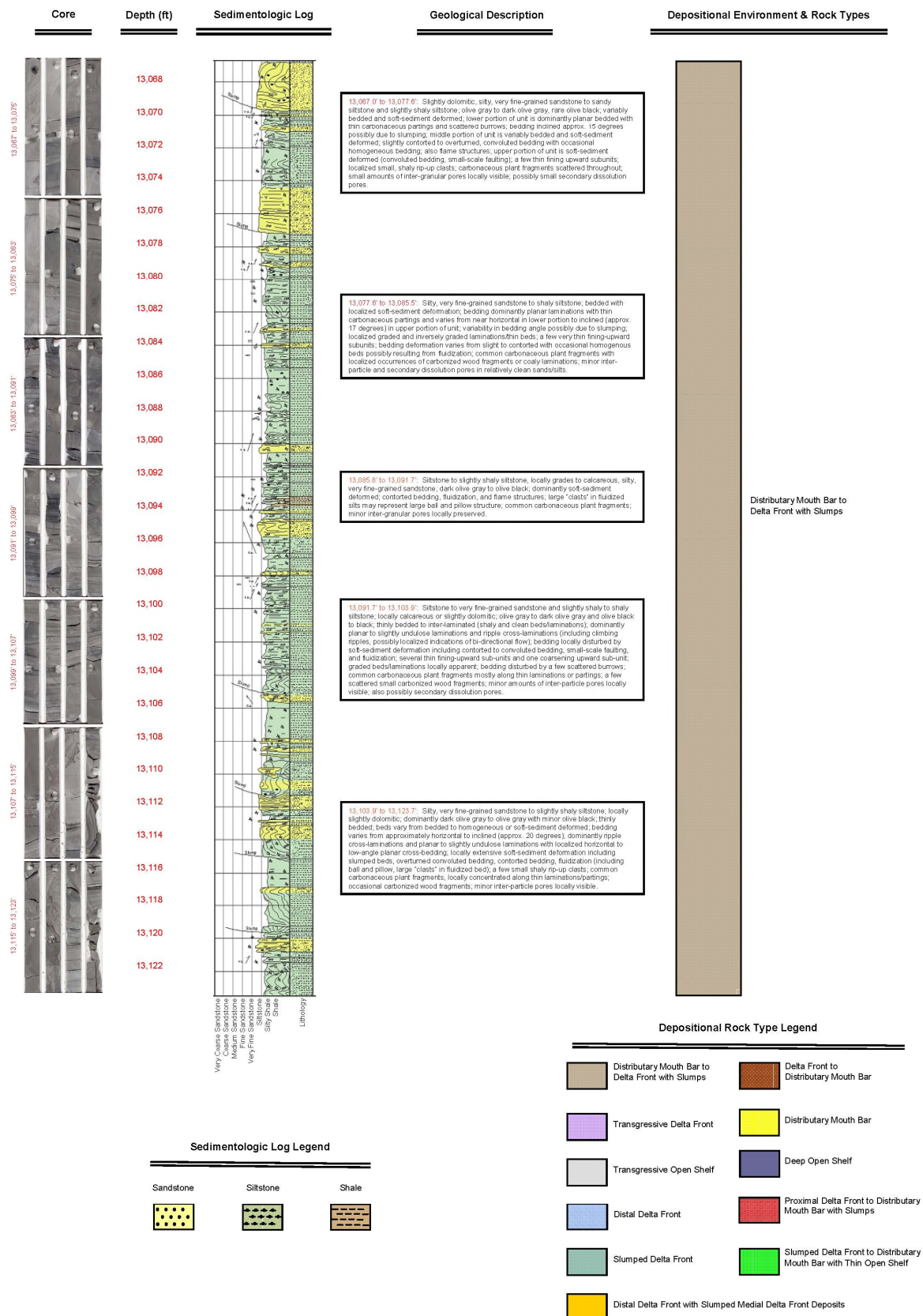


Fig. 5 — Core description, sedimentological log, and depositional environments and rock types for core No. 2 in the interval 13,067.0 ft to 13,123.5 ft, Upper York sands, ETX Well No. 1.

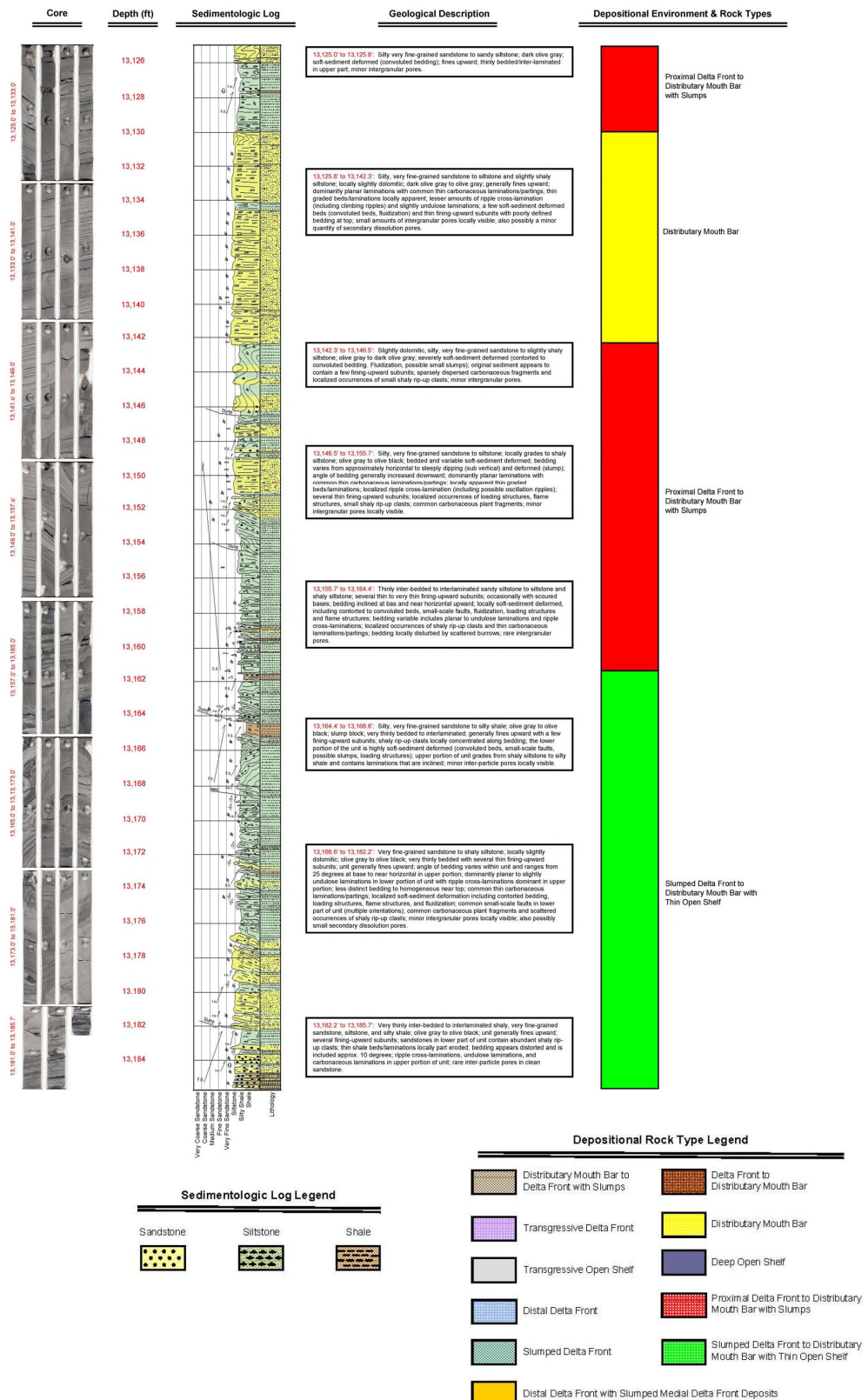


Fig. 6 — Core description, sedimentological log, and depositional environments and rock types for core No. 3 in the interval 13,125.0 ft to 13,185.7 ft, Middle York sands, ETX Well No. 1.

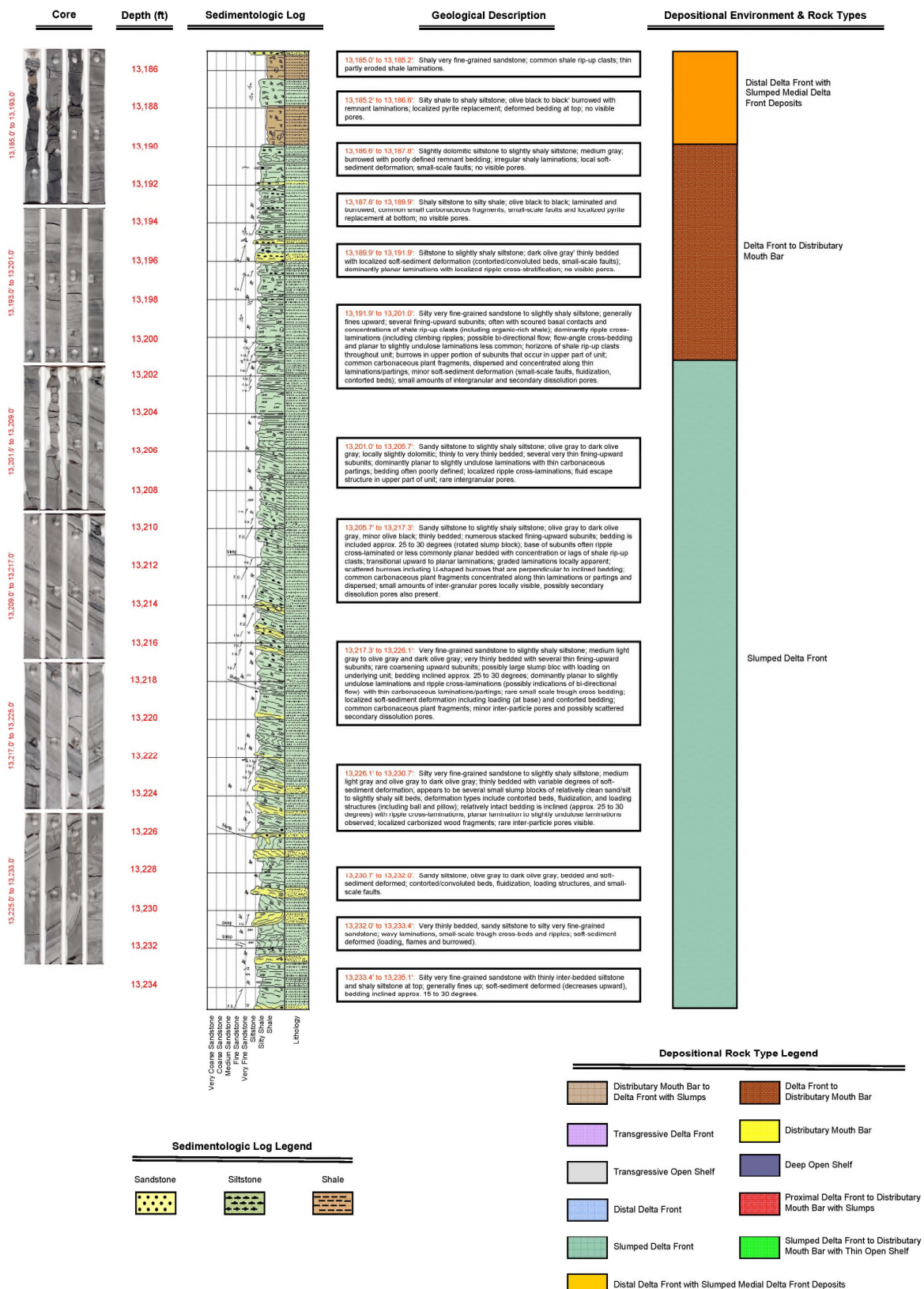


Fig. 7 — Core description, sedimentological log, and depositional environments and rock types for core No. 4 in the interval 13,185.0 ft to 13,235.1 ft, Bottom York sands, ETX Well No. 1.

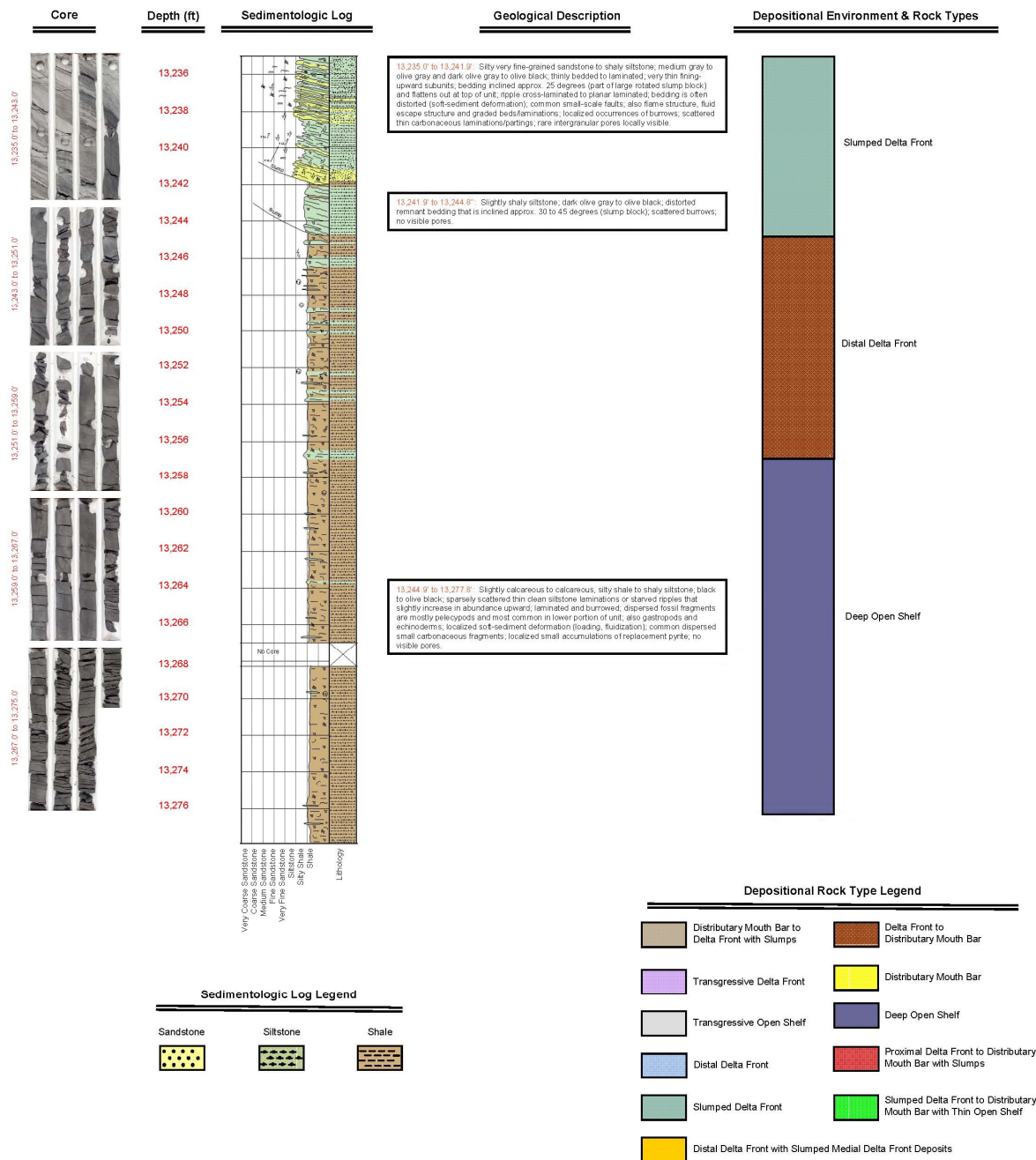


Fig. 8 — Core description, sedimentological log, and depositional environments and rock types for core No. 5 in the interval 13,235.0 ft to 13,277.8 ft, Bottom York sands, ETX Well No. 1.

All of the rock types show evidence of enhanced levels of compaction, including deformation of ductile grains (**Figs. 9c** and **9b**), elongate to slightly sutured grain contacts and stylolitic, organic-rich laminae (**Figs. 9a** and **9e**). Compaction can create a localized matrix (**Figs. 9d**) in the cleaner sandstones where argillaceous rock fragments are more abundant. In the more clay-rich sandstones, the high levels of compaction can make it difficult to distinguish detrital matrix clay from grain-derived pseudomatrix. As mentioned above, all samples have been magnified 125 times.

Mineralogy. Qualitative information from thin section petrography indicates that, in general, the detrital framework grains are largely comprised of quartz, followed by feldspar and rock fragments. Clay clasts are the most common type of rock fragment. Minor grain components include chert, mica, heavy minerals and organics. On the basis of the thin section analysis, the sandstones would appear to fall within the sublitharenite classification.

We also evaluated the whole rock and clay fraction mineralogy for eight of the samples (**Tables 4a and 4b**) using x-ray diffraction. Included are examples from each of the petrographic rock types. The three samples designated as clay-rich (PRT 4a, 4b, and 4c at depths of 13,034, 13,036 and 13,276 ft, respectively) average 57.2 percent quartz, 8.3 percent feldspar and 22 percent clay minerals. The quartz content for PRT 4c, lowest of the group at 51.8 percent, consists of both detrital grains and silicified shell fragments. The quartz, feldspar and clay mineral contents exhibit a surprisingly narrow range considering the variation in rock fabric observed petrographically. Calcite ranges from 6 to 9.4 percent and is highest in the samples containing the large skeletal fragments. Pyrite ranges from 1.3 to 3.9 percent, increasing as the amount of sand size material is reduced. Iron carbonates average less than 1 percent.

The argillaceous sandstones, represented by the samples from PRT 3b, PRT 3c and PRT 3f (depths of 13,148, 13,168 and 13,199 ft, respectively), average 70.2 percent quartz, 14.5 percent feldspar, and 14.8 percent clay. Only very minor amounts of other minerals are present. There is a trend of higher quartz and lower feldspar with increasing depth in the sandstones between 13,095 (PRT 2a) and 13,209 ft (PRT 1c). The highest quartz content (78.1 percent) is in the clean sandstone at 13,209 ft, which has 12 percent feldspar and 9.5 percent clay minerals. In comparison, the clean (calcite cemented) sandstone at 13,095 feet, is comprised of 57.3 percent quartz, 19.2 percent feldspar, and 20.7 percent calcite. The clay content for PRT 2a is very low at 2.3 percent. The clean sandstones have no detectable pyrite.

The total clay content of these sandstones includes clay held in grains (*i.e.* structural) as well as detrital matrix clay and diagenetic clay. Sandstones that contain higher concentrations of argillaceous rock fragments in laminae may have several percent of the measured clay in structural positions. The clay suite is consistently dominated by either illite or chlorite and these two clays combine to account for an average 90 percent of the clay present. A slightly expandable illite/smectite mixed-layer and kaolinite represent the other clay components. The relative abundance of the two dominant clay species does not appear to be related to any other rock property (*e.g.* texture, total clay content, porosity).

Table 4a — Bulk-Fraction Rock Mineralogy from X-Ray Diffraction Analysis

Sample	PRT 4a (percent)	PRT 4b (percent)	PRT 2a (percent)	PRT 3b (percent)	PRT 3c (percent)	PRT 3f (percent)	PRT 1c (percent)	PRT 4c (percent)
Mineralogy								
Quartz	58.6	61.2	57.8	69.6	68.9	72.2	78.1	51.8
K-Feldspar	0.6	0.6	0.4	0.4	0.3	0.3	0.2	0.7
Plagioclase	6.5	8.5	18.8	16.4	13.1	12.4	11.8	8.1
Calcite	9.0	6.0	20.7	0.0	0.3	0.0	0.0	9.4
Fe-Dolomite	0.2	0.2	0.0	0.0	0.2	0.0	0.2	0.3
Siderite	0.4	0.4	0.0	0.2	0.1	0.1	0.1	0.6
Pyrite	1.3	2.4	0.0	0.5	0.1	0.2	0.0	3.9
Clinoptilolite	1.2	1.1	0.0	0.1	0.1	0.0	0.0	1.1
Total Non-Clays	77.8	80.5	97.7	87.2	83.1	85.2	90.5	75.8
Illite/Smectite	1.2	0.9	0.2	0.4	0.5	0.2	0.4	0.7
Illite/Mica	4.5	8.0	0.9	6.6	4.0	7.5	3.3	11.0
Kaolinite	1.4	0.9	0.3	1.2	1.1	0.8	0.4	0.9
Chlorite	15.2	9.7	0.8	4.5	11.3	6.4	5.5	11.5
Total Clays	22.2	19.5	2.3	12.8	16.9	14.8	9.5	24.2

Table 4b — Clay-Fraction Rock Mineralogy from X-Ray Diffraction Analysis

Sample	PRT 4a (percent)	PRT 4b (percent)	PRT 2a (percent)	PRT 3b (percent)	PRT 3c (percent)	PRT 3f (percent)	PRT 1c (percent)	PRT 4c (percent)
Clay Mineralogy								
Illite/Smectite	5.2	4.8	9.1	3.4	2.8	1.4	3.8	3.0
Illite/Mica	20.2	40.8	41.4	51.8	23.7	50.4	34.2	45.6
Kaolinite	6.4	4.6	15.0	9.7	6.6	5.4	4.5	3.8
Chlorite	68.2	49.7	34.5	35.2	66.9	42.9	57.6	47.7

Diagenesis. Similar to most tight gas sands, the Bossier sands have been significantly modified by diagenesis. The most important forms of diagenesis (in order of frequency of occurrence and severity) are: mechanical compaction, cementation from quartz overgrowths, calcite cementation, grain-coating/pore lining clay development, grain dissolution, and ankerite cementation.

Mechanical compaction is the most prevalent form of diagenesis since it seems to have affected all of the rock types in the sample set. The enhanced level of compaction is most easily identified by the ductile grain deformation and elongate grain contacts evident in the clean sandstones. Grain deformation is recognized by argillaceous rock fragments that are squeezed into the adjacent primary pore space and effectively eliminating those pores. Contacts between more competent quartz grains tend to be elongate and slightly sutured which indicates grain rearrangement and a tighter packing configuration. The magnitude of the pore volume and pore aperture size reductions occurring with tighter packing have been shown to increase as grain size becomes more varied (*i.e.* with poorer sorting). The compaction that is most evident in the grain supported fabric has also occurred in the argillaceous rock types, including both the sandstones and claystones. The effect in these latter rock types is to compact the micro-fabric of the inter-granular and matrix clays, thereby reducing the inter-crystalline pore volume.

Quartz and calcite cementation, while potentially equally significant in terms of pore volume loss, appear to be restricted to the cleaner sandstones only. Quartz cementation, in the form of overgrowths, is extensive in the sandstones with limited inter-granular clay. The overgrowth crystals developing on adjacent grains tend to, coalesce and eventually link, thereby occluding the inter-granular pores. In the cleaner sandstones, quartz cement effectively destroys the primary pore system. No open inter-granular pores were evident in thin section (**Figs. 9a** and **9d**) and only scattered primary pore apertures are visible in the scanning electron photomicrographs (**Figs. 10a** and **10b**). Where present, the small open apertures are located adjacent to non-quartz framework grains and are preserved by the lack of overgrowth development. The argillaceous sandstones exhibit little or no quartz cement.

Calcite is a significant inter-granular cement in the clean sandstones at 13,095 ft (PRT 2a) and 13,121 ft (PRT 2b), and post dates compaction and the initial stage of quartz overgrowth development (**Figs. 9c** and **10c**). In these samples, the combination of calcite and quartz appears to be more detrimental than quartz cement alone. The inter-granular pore structure is more occluded (lacking even small open apertures — **Fig. 10d**) and secondary pore space is either not formed or is also calcite filled (grain replacement).

Diagenetic clay development is limited in the samples examined. Minor amounts of diagenetic chlorite and illite are present in the quartz-cemented sandstones and occur primarily as thin coatings on portions of the grain surfaces (predominantly non-quartz) and in association with the remnant pore throats (**Figs. 10a** and **10e**). A portion of the matrix clay has been recrystallized and currently displays diagenetic character in the argillaceous sandstones. This change in morphology is most noticeable in the rocks with higher porosity (*e.g.* PRT 3c) and chlorite appears to be the most affected clay (**Fig. 10f**). The matrix clay in the lower porosity samples at 13,148 ft (PRT 3b) and 13,199 ft (PRT 3f) has undergone less recrystallization (**Figs. 10g** and **10h**). Diagenetic clay is also located within the secondary pores in both the clean and argillaceous rocks, forming as an alteration product of the leached grains. These clays include fibrous illite (**Fig. 10i**) and mixtures of chlorite and illite (**Figs. 10j** and **10k**).

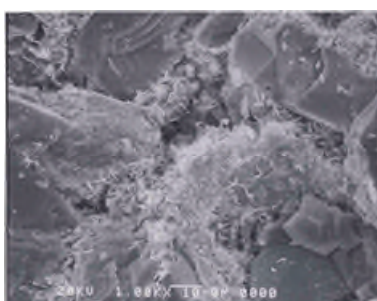


Fig. 10a — Sample PRT 1b (13,138 ft)

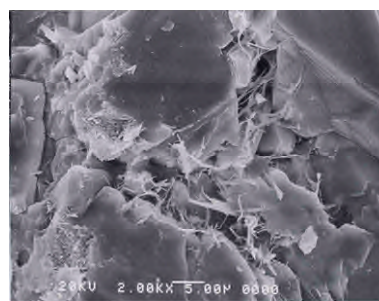


Fig. 10b — Sample PRT 1b (13,209 ft)



Fig. 10c — Sample PRT 1b (13,095 ft)

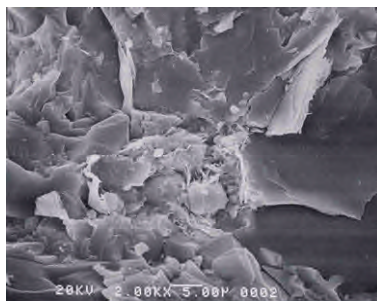


Fig. 10d — Sample PRT 1b (13,095 ft)

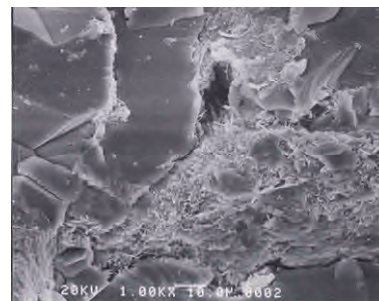


Fig. 10e — Sample PRT 1b (13,209 ft)

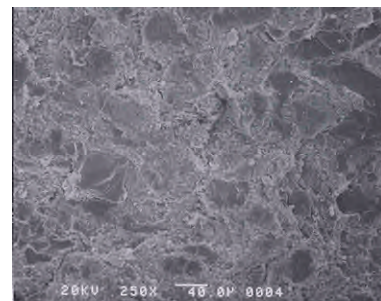


Fig. 10f — Sample PRT 1b (13,168 ft)

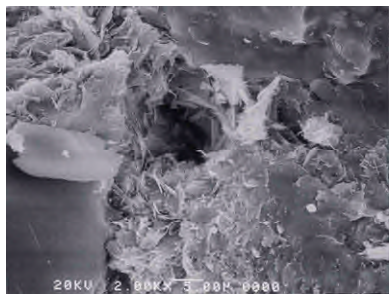


Fig. 10g — Sample PRT 1b (13,148 ft)

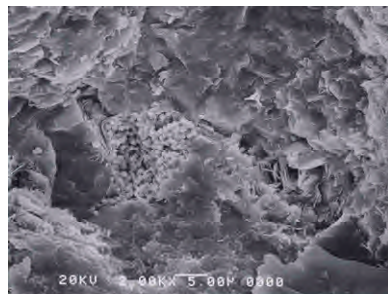


Fig. 10h — Sample PRT 1b (13,199 ft)

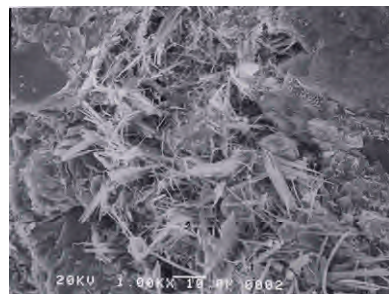


Fig. 10i — Sample PRT 1b (13,148 ft)

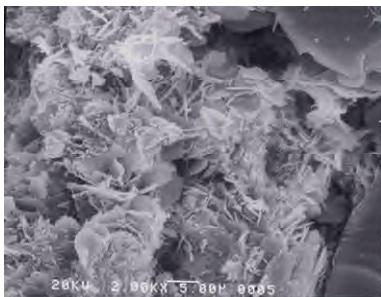


Fig. 10j — Sample PRT 1b (13,138 ft)



Fig. 10k — Sample PRT 1b (13,168 ft)

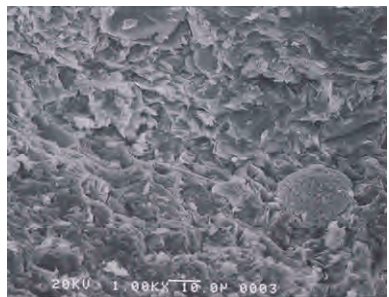


Fig. 10l — Sample PRT 1b (13,034 ft)

Minor grain dissolution has occurred in the quartz-cemented and argillaceous sandstones (**Figs. 9a** and **9d**). The grains affected include rock fragments and feldspar. Dissolution is rarely complete and remnant material is commonly converted to diagenetic clay, which limits the pore volume contributed by this process.

Finally, ankerite and pyrite represent only minor diagenetic components. The ankerite occurs as an isolated cement and may also develop as a grain replacement (**Figs. 9d** and **9f**). Pyrite is absent in the cleaner sandstones, but occurs in the other rock types such as framboids embedded in the detrital clay (**Figs. 10h** and **10l**). Neither mineral significantly impacts the preservation or development of pore space.

Pore Structure from Mercury-Injection Capillary Pressure Measurements. Capillary pressure measurements using mercury injection show differences in the type and distribution of pore space for the samples tested. These differences exist because of the variations in depositional texture (*i.e.* clean vs. argillaceous), as well as because of diagenetic alteration. However, all of the samples have pore structures that fall in the micro-porous range with pore apertures that are less than 1 micron diameter (see **Table 3**). The capillary pressure data show that, within each of the petrographic rock types, the pore structures exhibit some degree of similarity. Characteristic capillary pressure curves for the low porosity, clay-rich rocks (**Fig. 11b**) have a poorly defined intrusion profile, and the median aperture size is generally less than 0.01 microns (diameter). The porosity (probably compacted micro-fabric) is held within the inter-crystalline pores of the matrix clay.

The cleaner sandstones (both with and without calcite cement) tend to have uni-modal pore aperture distributions (**Fig. 11a**) which is interpreted as domination by the remaining inter-granular pore system. Compaction and extensive cementation patterns have reduced inter-granular pore remnants into a size range normally ascribed to clay-related micropores. The location of the intrusion maximum is below 0.10 micron for the calcite-cemented rocks (PRT 2) and in the 0.10 to 0.30 micron range for quartz-cemented sandstones (PRT 1). Median aperture sizes (diameter) are, on average, 0.05 microns for the calcite-cemented samples and 0.22 microns for the more porous quartz-cemented rock. Several of the pore aperture distribution curves also show subtle tails towards the smaller apertures that can be indicative of a clay effect. The current pore structure includes a limited amount of secondary (diagenetic) pore space formed by grain dissolution. These pores are connected only to the primary inter-granular system and are not reflected in the pore aperture size distribution profiles. However, secondary pore space does impact the total porosity.

The samples grouped as grain-supported, argillaceous sandstones (PRT 3) display the most variability. All of the pore volume is assumed to be held as inter-crystalline micro-pores associated with the detrital and diagenetic (recrystallized) clay. The average median apertures size (diameter) is 0.06 microns with a range from 0.013 to 0.123 microns. Laboratory measurements suggest these differences in aperture size are related to the amount of clay and/or clay diagenesis. The remaining argillaceous sandstones have less well-defined pore structures as shown by the capillary pressure curve shapes. Intrusion profiles tend to be broad without obvious maximums. This latter subgroup is characterized by a more heterogeneous fabric partially marked by subtle variations in the matrix clays. The observed differences may be related to depositional (*e.g.*, suspension versus gravity driven) or post-depositional processes (*e.g.*, burrowing). These differences could affect the texture and clay micro-fabric (*e.g.* particle orientation), and therefore the response to compaction.

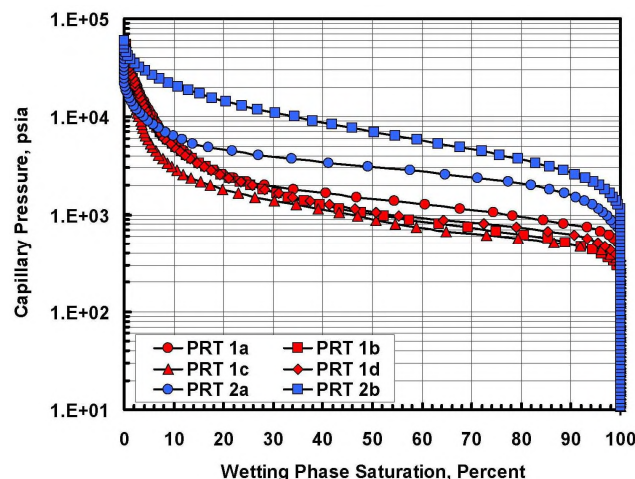


Fig. 11a — Mercury-injection capillary pressure data, petrographic rock types 1 and 2.

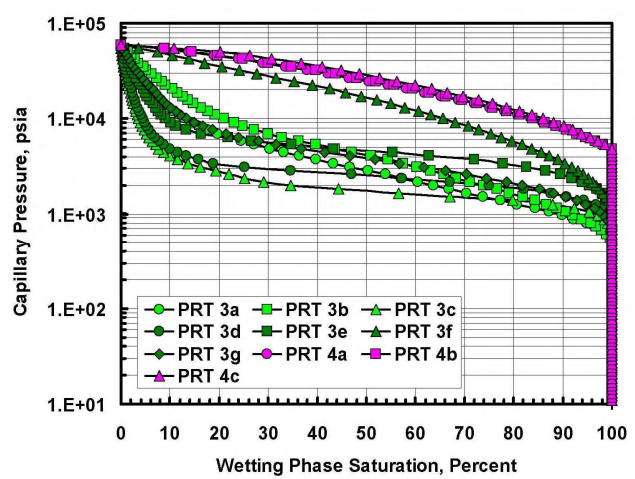


Fig. 11b — Mercury-injection capillary pressure data, petrographic rock types 3 and 4.

Comparing Petrographic and Depositional Rock Types. We have also compared the depositional rock types and environments with the petrographic rock type samples from the corresponding intervals. Inspection of the results in **Table 5** shows that eight (8) different *depositional* rock types appear within the four (4) *petrographic* rock type classifications. This comparison illustrates that there is either no unique relationship or only a very poor correlation between the depositional environment and the post-depositional rock characteristics. For example, *petrographic rock type 3 has been identified in five (5) different depositional rock types*. This comparison demonstrates not only how diagenesis can alter the original rock properties present at deposition, but also how difficult it is to predict rock quality from just the depositional environment. In short, *the range of depositional rock types represented by each petrographic rock type in this well suggests rock quality cannot be predicted accurately using rock properties expected from a particular depositional environment*.

Table 5 — Comparison of Representative Petrographic Rock Types and Their Associated Depositional Rock Types

Petrographic Rock Type No.	Sample Depth (ft)	Depositional Rock Type No.	Depositional Rock Type Description
1a	13,112	6	Distributary mouth bar to delta front with slumps
1b	13,138	8	Distributary mouth bar
1c	13,209	3	Slumped delta front
1d	13,221	3	Slumped delta front
2a	13,095	6	Distributary mouth bar to delta front with slumps
2b	13,121	6	Distributary mouth bar to delta front with slumps
3a	13,131	8	Distributary mouth bar
3b	13,148	7	Proximal delta front to distributary mouth bar with slumps
3c	13,168	9	Slumped delta front to distributary mouth bar with thin open shelf
3d	13,171	9	Slumped delta front to distributary mouth bar with thin open shelf
3e	13,176	9	Slumped delta front to distributary mouth bar with thin open shelf
3f	13,199	5	Delta front to distributary mouth bar
3g	13,203	3	Slumped delta front
4a	13,034	1	Distal delta front
4b	13,036	1	Distal delta front
4c	13,276	11	Deep open shelf

Hydraulic Rock Types, ETX Well No. 1. The final step in our rock typing work-flow process is identification of hydraulic rock types (HRT). We have employed the Winland/Pittman method [Pittman, 1992b] to classify hydraulic rock types using routine permeability-porosity data combined with mercury-injection capillary pressure measurements from core plugs. Horizontal plugs were obtained from the conventional whole core using a sampling interval of one foot. In some cases, we obtained additional plugs in order to capture specific rock features not represented by the sampling interval.

All plugs were then cleaned using a low-temperature, cold solvent method (*i.e.*, a mixture of toluene and methanol) and dried in a humidified oven at a temperature of 145 Deg F. Both cleaning and drying techniques were designed to minimize clay damage and alteration of physical rock properties [Soeder, 1986; Luffel, *et al.*, 1990; and Morrow, *et al.*, 1991]. We then measured effective porosity and absolute permeability using a minimum net confining pressure of 800 psig. Effective porosity was measured using a gas expansion method (with helium) and absolute permeability was measured using an unsteady-state technique.

The first, and the most critical, step in the Winland/Pittman method is identification and quantification of the dominant pore throat dimensions. The principle underlying this method is that the pore throats, rather than the overall pore volume (*i.e.*, porosity), control flow capacity in reservoir rock. In other words, porosity alone is not an accurate predictor of rock quality, especially in low-permeability sands with significant diagenesis. However, we should be able to develop unique permeability-porosity relationships for hydraulic rock types that have been grouped according to the dominant pore throat dimension.

To quantify the dominant pore throat dimension, we employed mercury-injection capillary pressure data in which we plot pore throat radius (computed from the capillary pressure measurements) against incremental mercury saturation. Using the mercury-injection capillary pressure data from the petrographic rock typing stage, as well as supplemental measurements for other core samples, we have identified five (5) different *hydraulic* rock types (**Fig. 12a**) that have been grouped according to the following pore throat radius range:

- Hydraulic Rock Type 1 (HRT 1): $r > 0.25$ microns (best reservoir rock)
- Hydraulic Rock Type 2 (HRT 2): $0.10 \text{ microns} < r \leq 0.25$ microns (medium/high-quality reservoir rock)
- Hydraulic Rock Type 3 (HRT 3): $0.05 \text{ microns} < r \leq 0.10$ microns (medium-quality reservoir rock)
- Hydraulic Rock Type 4 (HRT 4): $0.03 \text{ microns} < r \leq 0.05$ microns (low-quality reservoir rock)
- Hydraulic Rock Type 5 (HRT 5): $0.03 \text{ microns} \leq r$ microns (non-reservoir rock)

Next, we investigated permeability-porosity relationships for each hydraulic rock type. For this, we used the Winland/Pittman equations [Kolodzie, 1980; Pittman, 1992b] which relate absolute permeability to effective porosity as a function of the dominant pore throat radius. The appropriate equation may be determined from characteristics of an "apex plot" which graphs mercury saturation divided by capillary pressure on the *y*-axis versus mercury saturation on the *x*-axis. The inflection point represents the maximum pore throat radius as a function of mercury saturation. This pore throat dimension has been used by Winland/Pittman [1992b] as an effective correlating parameter for an empirical porosity-permeability relation. For example, the r_{35} designation refers to the pore throat radius corresponding to the 35th percentile mercury saturation on a plot of cumulative percent pore space saturated by mercury against the logarithm of pore throat radius.

The "apex plot" for ETX Well No. 1 is shown in **Fig. 12b**. Except for the very low-quality rock samples, the majority of the curve shapes have apexes between 20 and 30 percent mercury saturation. As such, we have chosen to use the porosity-permeability correlation developed for the 25th percentile of saturation [Pittman, 1992b]

$$\log r_{25} = 0.204 + 0.531 \log k - 0.350 \log \phi , \dots \quad (5)$$

where r_{25} is the pore throat radius (microns), k is the absolute permeability (md), and ϕ is the effective porosity (percent). Note that the original correlations were developed primarily using permeabilities to air (*i.e.*, permeability measurements uncorrected for gas slippage). However, we use Klinkenberg-corrected values in our rock typing approach.

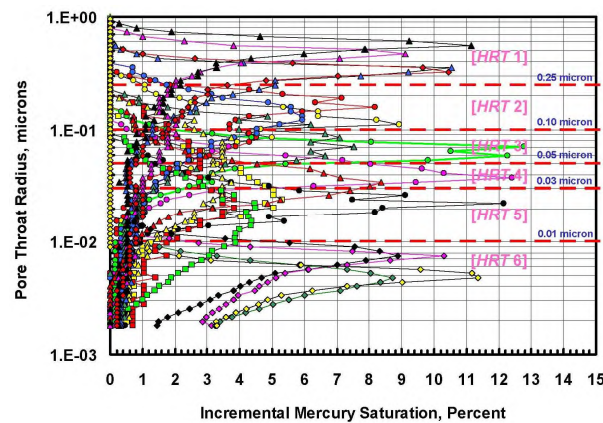


Fig. 12a — Identification of hydraulic rock types from dominant pore throat dimensions.

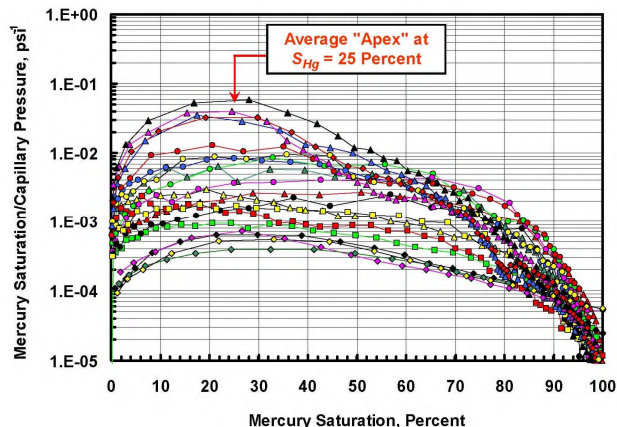


Fig. 12b — "Apex plot" showing maximum pore throat radius at mercury saturation of 25 percent.

Next, we constructed a semilog plot (**Fig. 13**) of absolute Klinkenberg-corrected permeability against effective porosity for all core measurements. We superimposed the Pittman [1992b] r_{25} permeability-porosity correlations given by Eq. 5 for dominant pore throat radii of 1.0, 0.25, 0.10, 0.05, and 0.03 microns. Note that hydraulic rock type 5 is not plotted since these are essentially non-reservoir rocks. The groupings of data points located within each ellipse represent the range of permeability and porosity for each hydraulic rock type. The ellipse located on the far left of the plot represents core samples that were artificially fractured during the coring process and are not included in any of the hydraulic rock type classifications. We observe that each rock type is defined by a broad range of porosity values but a rather narrow range of permeabilities.

Comparing Depositional and Petrographic Rock Types with Hydraulic Rock Types. Figures 14a and 14b are semilog plots of the Klinkenberg-corrected permeability plotted against the effective porosity for depositional and petrographic rock types, respectively. Each of the rock property data sets has been grouped and identified according to the various depositional and petrographic rock types defined previously. Again, superimposed on these plots are the hydraulic rock type ellipses (identified in Fig. 13) and the Pittman [1992b] r_{25} permeability-porosity correlations (given by Eq. 5) for dominant pore throat radii of 1.0, 0.25, 0.10, 0.05, and 0.03 microns. Any correlation will be indicated by significant clusters of permeability-porosity data points from depositional or petrographic rock types within each of the hydraulic rock type ellipses.

Not surprisingly, we see no clear, unique correlation between depositional and hydraulic rock types in Fig. 14a. Most depositional rock types have permeability and porosity values representative of and encompassing all four hydraulic rock types. Closer inspection of Fig. 14a does, however, reveal some very subtle patterns (but very poor correlations). For example, rock properties for depositional rock type 3 (slumped delta front) seem to match hydraulic rock types 2 and 3, while depositional rock type 5 (delta front to distributary mouth bar) fall primarily in the region for hydraulic rock types 1 and 2. The existence of any correlation between depositional and hydraulic rock types (albeit very poor) is probably indicative of some of the underlying characteristics from the original depositional processes.

Although the data set is smaller, we see slightly better correlation between some petrographic and hydraulic rock types in Fig. 14b. The best petrographic rock types (PRT 1) are clustered in the ellipses for hydraulic rock types 1 and 2, also representing the best quality rocks. Similarly, the worst petrographic rock types (PRT 4) are grouped in the ellipse for the poorest reservoir rock represented by hydraulic rock type 4. Surprisingly, the second best petrographic rock type data sets (PRT 2, as identified from microscopic imaging) are located in the ellipse for hydraulic rock type 4 (representing low-quality reservoir rock). Moreover, the permeability-porosity measurements for petrographic rock type 3 span the entire range of hydraulic rock types, indicating no correlation.

Similar conclusions can be drawn from the data trends shown in Figs. 15a and 15b for depositional rock types and Figs. 16a and 16b for the petrographic rock types. For example, the Klinkenberg-corrected absolute permeability estimates are grouped and plotted in Fig. 15a according to depositional rock type. We observe two important data trends. First, the rock permeability extends over three orders of magnitude for all rock types. Secondly, the range of permeability values is almost identical regardless of the depositional environment which again suggests there is no permeability correlation by depositional rock type.

We see similar trends for effective porosity in Fig. 15b. Although there are fewer data points and the value range is not as significant, we can arrive at similar conclusions for the petrographic rock type data shown in Figs. 16a and 16b.

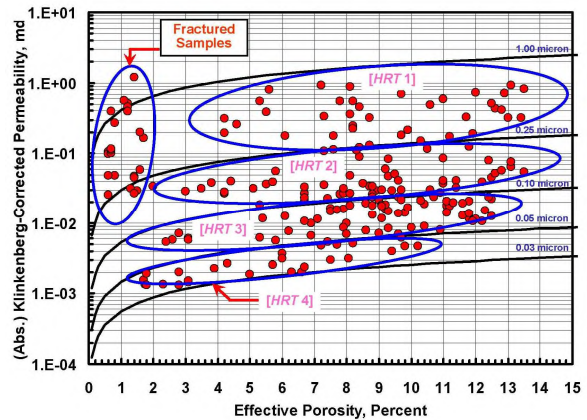


Fig. 13 — Winland semilog plot of permeability against porosity for various *hydraulic* rock types.

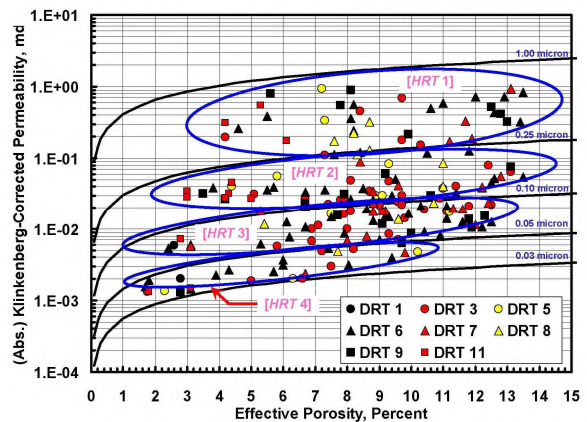


Fig. 14a — Winland plot showing relationship between depositional and *hydraulic* rock types.

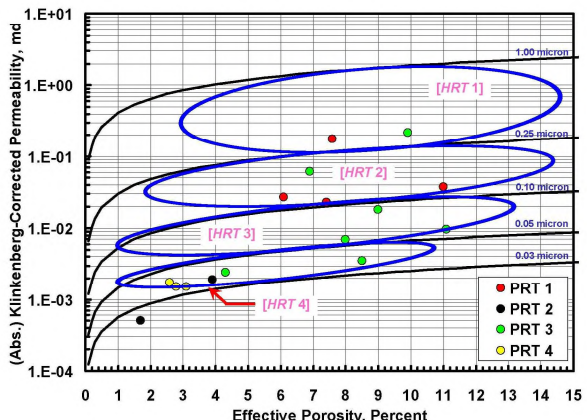


Fig. 14b — Winland plot showing relationship between petrographic and *hydraulic* rock types.

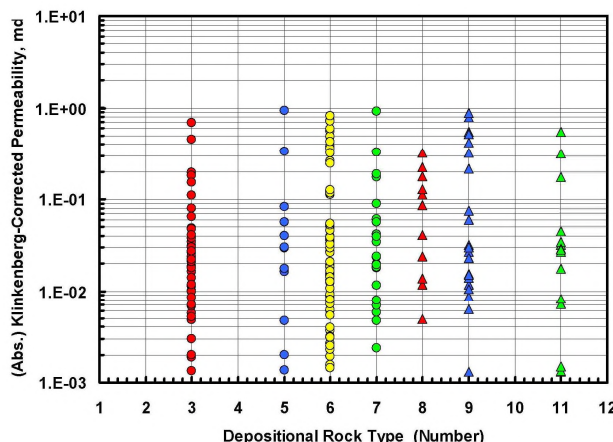


Fig. 15a — Range of absolute permeability by depositional rock type.

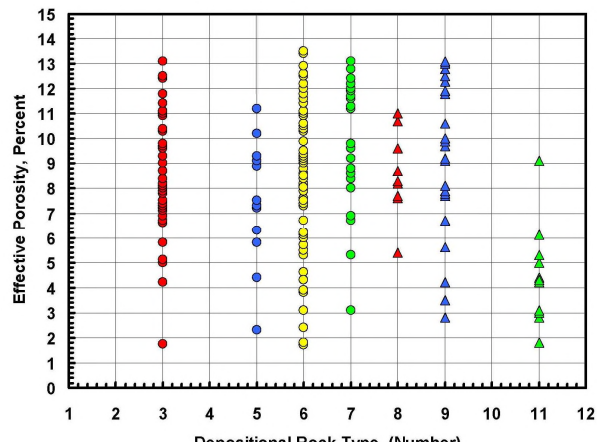


Fig. 15b — Range of effective porosity by depositional rock type.

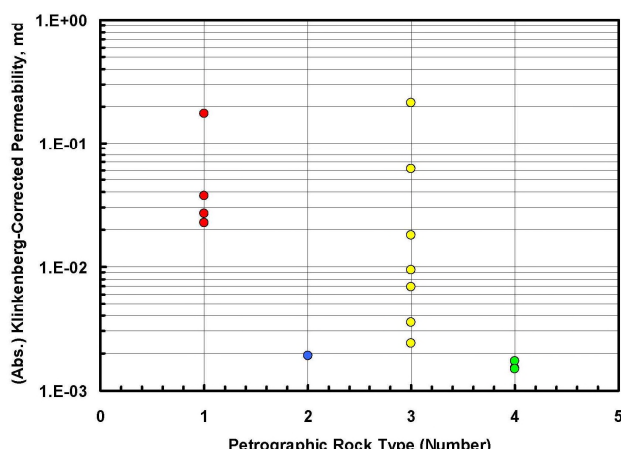


Fig. 16a — Range of absolute permeability by petrographic rock type.

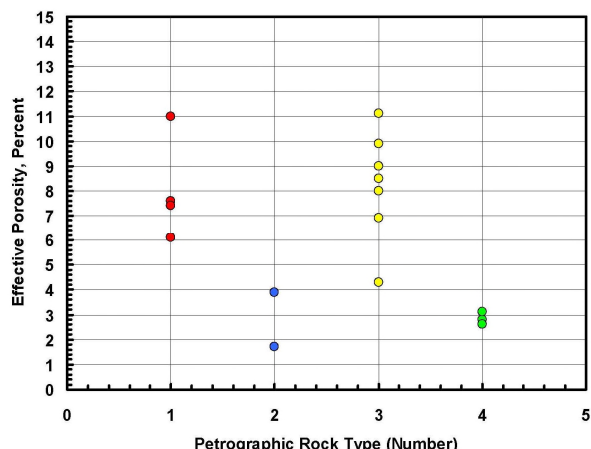


Fig. 16b — Range of effective porosity by petrographic rock type.

Summary and Conclusions

We have developed a work-flow process that provides a consistent procedure to systematically integrate both large-scale geologic elements and small-scale rock petrology with the physical rock flow and storage properties in low-permeability sandstone reservoirs. Our work-flow process uses a core-based, rock typing approach that is developed to capture rock properties characteristic of tight gas sands. Fundamental to this process are identification and comparison of three different rock types — *depositional*, *petrographic*, and *hydraulic*.

Each rock type represents different physical and chemical processes affecting rock properties during the depositional and para-genetic cycles. Most tight gas sands have been subjected to post-depositional diagenetic events, so a comparison of all three rock types will allow us to assess the impact of diagenesis on the physical rock properties. If the effects of diagenesis are minor, we would expect to observe the permeability-porosity relationships derived for depositional rock types (using expected rock properties derived from geologic models of the depositional environments and processes) to be applicable to both petrographic and hydraulic rock types.

However, as the effects of diagenesis increase in severity, magnitude, and occurrence, the original rock texture and composition, pore geometry, and physical rock properties will be modified. Under these conditions, we would expect to see little or no correlation of permeability-porosity relationships derived for each of the different rock types. And more importantly, use of the depositional environment and the associated (depositional) rock types to guide field development activities is likely to result in ineffective and inefficient exploitation.

We have also illustrated application of our rock-typing work-flow process with an example from the Bossier tight gas sand play from a producing field in Freestone County, Texas in the East Texas Basin. On the basis of the results from the field example, we offer the following conclusions:

1. The Bossier tight gas sands (as represented by the example shown in this paper) have been subjected to significant post-depositional diagenesis. Although much of the reservoir interval has retained some underlying traits of the ori-

- ginal depositional conditions, the physical rock properties have been altered significantly.
2. The depositional environment (*i.e.*, the expected rock properties derived from geologic models of the depositional environments and processes) and the associated rock types are poor predictors of reservoir quality. *We have observed no unique permeability-porosity relationships for any of the depositional rock types identified in the example well.* In fact, all of the depositional rock types exhibit the same broad range of properties.
 3. *Although there are slightly better permeability-porosity relationships using petrographic rather than depositional rock types, we still do not observe strong or unique correlations.* Petrographic rock types are derived from qualitative descriptions of the rocks, and it is important to understand the processes affecting rock properties. However, we still need *physical* or *quantitative* property measurements — especially absolute permeability and effective porosity.
 4. When grouped according to the dominant pore throat dimensions, we observe distinct collections or groupings of rocks and their associated properties (*i.e.*, the hydraulic rock types). These groupings (or typings) of rocks will allow us to develop unique permeability-porosity correlations for each hydraulic rock type.
 5. *Each of the hydraulic rock types identified from our rock typing study extends over a rather narrow range of absolute permeability values.* However, the range of effective porosity values covered by each hydraulic rock type suggests porosity is not necessarily a good indicator of reservoir quality (*e.g.*, porosity alone is not an accurate delimiter for recognizing net pay in tight gas sands).

Acknowledgments

We would like to express our thanks to Anadarko Petroleum Corp. for permission to publish this paper and for permission to use the field data to illustrate the rock typing process. We would also like to acknowledge Mr. George Bolger (Petro-Tech Associates) for his petrographic analysis and Mr. Peter Purazzella (OMNI Laboratories, Inc.) for his geological interpretations and core descriptions.

Nomenclature

Field Variables:

b	=	gas slippage factor, atm
dp/dx	=	pressure gradient, psi/cm
k	=	absolute permeability, md
k_∞	=	Klinkenberg-corrected permeability, md
\bar{p}	=	average or arithmetic mean pressure, atm
r	=	radius of rock pore throat aperture, microns
v_x	=	interstitial gas velocity, cm/sec

Greek Variables:

β	=	Forchheimer inertial resistance coefficient, cm^{-1}
ϕ	=	effective permeability to gas, percent
μ	=	average gas viscosity, cp
ρ	=	gas density, g/cm^3

References

1. Acosta, L., *et al.*: "Reservoir Study V9 of El Furrial Field, Venezuela," paper SPE 95047 presented at the SPE Latin American and Caribbean Petroleum Engineering Conference (2005), Rio de Janeiro, Brazil, June 20-23.
2. Al-Aruri, A., *et al.*: "Rock Type and Permeability Prediction from Mercury Injection Data: Application to a Heterogeneous Carbonate Oil Reservoir, Offshore Abu Dhabi (United Arab Emirates)," presented at the 8th SPE Abu Dhabi International Petroleum Exhibition and Conference (1998), Abu Dhabi, U.A.E., October 11-14.
3. Al-Farisi, O., *et al.*: "Electrical Resistivity and Gamma Ray Logs: Two Physics for Two Permeability Estimation Approaches in Abu Dhabi Carbonates," paper SPE 88687 presented at the 11th SPE Abu Dhabi International Petroleum Exhibition and Conference (2001), Abu Dhabi, U.A.E., Oct. 10-13.
4. Al-Habshi, A., *et al.*: "Application of Sequence Stratigraphy and Petrography in Preparation of Reservoir Rock Typing Scheme in One of Thamama Gas Reservoirs of Onshore Abu Dhabi," paper SPE 81533 presented at the 13th SPE Middle East Oil Show & Conference, Bahrain (2003), June 9-12.
5. Ali-Nandalal, J. and Gunter, G.: "Characterizing Reservoir Performance for the Mahogany 20 Gas Sand Based on Petrophysical and Rock Typing Methods," paper SPE 81048 presented at the SPE Latin American and Caribbean Petroleum Engineering Conference (2003), Port-of-Spain, Trinidad, West Indies, Apr. 27-30.
6. Amyx, J.W., Bass, D.M., Jr., and Whiting, R.L.: *Petroleum Reservoir Engineering: Physical Properties*, McGraw-Hill Book Co., New York, NY (1960).
7. Aplin, G.F., *et al.*: "New Insights From Old Data: Identification of Rock Types and Permeability Prediction Within a Heterogeneous Carbonate Reservoir Using Diplog and Openhole Log Data," paper SPE 78501 presented at the 10th SPE Abu Dhabi International Petroleum Exhibition and Conference (2002), Abu Dhabi, U.A.E., Oct. 13-16.
8. Archie, G.E.: Introduction to Petrophysics of Reservoir Rocks," *AAPG Bull.* (1950) vol. 34, 943-961.

9. Beiranvand, B.: "Quantitative Characterization of Carbonate Pore Systems by Mercury-Injection Method and Image Analysis in a Homogeneous Reservoir," paper SPE 81479 presented at the 13th SPE Middle East Oil Show & Conference (2003), Bahrain, Apr. 5-8.
10. Berg, R.R.: *Sandstone Reservoirs*, Prentice-Hall, Englewood Cliffs, NJ (1986).
11. Boada, E., et al.: "Rock Typing: Key Approach for Maximizing Use of Old Well Log Data in Mature Fields, Santa Rosa Field, Case Study," paper SPE 69459 presented at the SPE Latin American and Caribbean Petroleum Engineering Conference (2001), Buenos Aires, Argentina, March 25-29.
12. Bloch, S., Lander, R.H., and Bonnell, L.: "Anomalously High Porosity and Permeability in Deeply Buried Sandstone Reservoirs: Origin and Predictability," *AAPG Bull.*, vol. 86, no. 2 (2002) 301-328.
13. Creusen, A., et al.: "Property Modeling Small Scale Heterogeneity of Carbonate Facies," paper SPE 111451 presented at the SPE/EAGE Reservoir Characterization and Simulation Conference (2007), Abu Dhabi, U.A.E., October 28-31.
14. Davies, D.K.: "Image Analysis of Reservoir Pore Systems: State of the Art in Solving Problems Related to Reservoir Quality," paper SPE 19407 presented at the SPE Formation Damage Control Symposium (1990), Lafayette, LA, Feb. 22-23.
15. Davies, K.K., Williams, B.P.J., and Vessell, R.K.: "Reservoir Geometry and Internal Permeability Distribution in Fluvial, Tight Gas Sandstones, Travis Peak Formation, Texas," paper SPE 21850 presented at the Rocky Mountain Regional Meeting and Low-Permeability Reservoirs Symposium (1991), Denver, CO, April 15-17.
16. Davies, D.K., Vessell, R.K., and Auman, J.B.: "Improved Prediction of Reservoir Behavior Through Integration of Quantitative Geological and Petrophysical Data," *SPE Reservoir Evaluation & Engineering* (April 1999), 149-160.
17. Dibble, W.E., Jr., Nur, A., and Potter, J.M.: "Porosity Reduction in Sandstone," paper SPE 11970 presented at the 58th SPE Annual Technical Conference and Exhibition (1983), San Francisco, CA, October 5-8.
18. Fancher, G.H., et al.: "Some Physical Characteristics of Oil Sands," *Bull. 12*, Pennsylvania State C., Minerals Industries Experiment Station, University Park, PA (1933), **65**.
19. Forchheimer, P.: "Wasserbewegung durch Boden," *Zeitz ver Deutsch Ing.* (1901) **48**, 1731.
20. Frank, S., et al.: "Carbonate Rock Typing Using NMR Data: A Case Study from Al Shaheen Field, Offshore Qatar," paper IPTC 10889 presented at the SPE International Petroleum Technology Conference (2005), Doha, Qatar, November 21-23.
21. Green, L. and Duwez, P.: "Fluid Flow Through Porous Metals," *J. Applied Mech.* (1951) 39-45.
22. Grotsch, J., Al-Jelani, O., and Al-Mehairi, Y.: "Integrated Reservoir Characterization of a Giant Lower Cretaceous Oil Field, Abh Dhabi, U.A.E." paper SPE 49454 presented at the 8th SPE Abu Dhabi International Petroleum Exhibition and Conference, (1998) Abu Dhabi, U.A.E., October 11-14.
23. Geertsma, J.: "Estimating the Coefficient of Inertial Resistance in Fluid Flow Through Porous Media," *Soc. Pet. Eng. J.* (1974), 445-450.
24. Gunter, G.W., et al.: "Overview of an Integrated Process Model to Develop Petrophysical Based Reservoir Descriptions," paper SPE 38748 presented at the SPE Annual Technical Conference and Exhibition (1997a), San Antonio, TX, Oct. 5-8.
25. Gunter, G.W., et al.: "Early Determination of Reservoir Flow Units Using an Integrated Petrophysical Method," paper SPE 38679 presented at the SPE Annual Technical Conference and Exhibition (1997b), San Antonio, TX, Oct. 5-8.
26. Guo, G., et al.: "Rock Typing as an Effective Tool for Permeability and Water-Saturation Modeling: A Case Study in a Clastic Reservoir in the Oriente Basin," paper SPE 97033 presented at the SPE Annual Technical Conference and Exhibition (2005), Dallas, TX, October 9-12.
27. Holland, M.T.: "Reservoir Property Implications of Pore Geometry Modification Accompanying Sand Diagenesis: Anahuac Formation, Louisiana," paper SPE 10991 presented at the 57th Annual Fall Technical Conference and Exhibition of the Society of Petroleum Engineers (1982), New Orleans, LA, September 26-29.
28. Huet, C.C., et al.: "A Modified Purcell/Burdine Model for Estimating Absolute Permeability from Mercury-Injection Capillary Pressure Data," paper IPTC 10994 presented at the IPTC International Petroleum Technology Conference (2005), Doha, Qatar, Nov. 21-23.
29. Hunt, J.M., "Generation and Migration of Petroleum from Abnormally Pressured Fluid Compartments", *AAPG Bull.*, (1990) vol. 74, no.1, 1-12.
30. Johnson, T.W. and Taliaferro, D.B.: "Flow of Air and Natural Gas Through Porous Media," *Technical Paper 592*, USBM (1938).
31. Jones, S.C., "A Rapid Accurate Unsteady-State Klinkenberg Permeameter," *Soc. Pet. Engr. J.* (1972), 383-397.
32. Jones, S.C.: "A Technique for Faster Pulse-Decay Permeability Measurements in Tight Rocks," paper SPE 28450 presented at the SPE Annual Technical Conference and Exhibition (1994), New Orleans, LA, Sept. 25-28.
33. Katz, D.L., et al.: *Handbook of Natural Gas Engineering*, McGraw-Hill Publishing Co., New York, NY (1959), pp 46-51.
34. Keelan, D.K.: "Automated Core Measurement System for Enhanced Core Data at Overburden Conditions," paper SPE 15185 presented at the SPE Rocky Mountain Regional Meeting (1986), Billings, MT, May 19-21.
35. Keighin, C.W. and Sampath, K.: "Evaluation of Pore Geometry of Some Low-Permeability Sandstones Uinta Basin," *J. Pet. Tech.* (Jan. 1982) 65-70.
36. Klinkenberg, L.J.: "The Permeability of Porous Media to Liquids and Gases," *API Drilling and Production Practices* (1941) 200-213.
37. Kolodzie, S., Jr.: "Analysis of Pore Throat Size and Use of the Waxman-Smits Equation to Determine OOIP in Spindle Field, Colorado," paper SPE 9382 presented at the 1980 55th Annual Fall Technical Conference and Exhibition of the Society of Petroleum Engineers, Dallas, TX, Sept. 21-24.
38. Law, B.E. 2000, "What Is A Basin-Centered Gas System?," in 2000 Basin-Center Gas Symposium, Rocky Mountain Association of Geologists, Denver, Colorado (Oct. 6).
39. Leal, et al.: "Bimodal Behavior of Mercury-Injection Capillary Pressure Curve and Its Relationship to Pore Geometry, Rock Quality and Production Performance in a Laminated and Heterogeneous Reservoir," paper SPE 69457 presented at the 2001 SPE Latin American and Caribbean Petroleum Engineering Conference, Buenos Aires, Argentina, Mar. 25-28.
40. Lee, S.H., Kharghoria, A., and Datta-Gupta, A.: "Electrofacies Characterization and Permeability Predictions in Complex Reservoirs," *SPE Reservoir Evaluation & Engineering* (June 2002), 237-248.

41. Luffel, D.L. and Howard, W.E.: "Reliability of Laboratory Measurement of Porosity in Tight Gas Sands," *SPE Formation Eval.* (1988) 705-710.
42. Luffel, D.L., Herrington, K.L., and Walls, J.D.: "Effect of Extraction and Drying on Flow, Capillary, and Electrical Properties of Travis Peak Cores Containing Fibrous Illite," paper SPE 20725 presented at the 65th Annual Technical Conference and Exhibition of the Society of Petroleum Engineers (1990), New Orleans, LA, Sept. 23-26.
43. Luffel, D.L., Herrington, K.L., and Harrison, C.W.: "Fibrous Illite Controls Productivity in Frontier Gas Sands, Moxa Arch, Wyoming," paper SPE 21876 presented at the 1991 SPE Rocky Mountain Regional Meeting and Low-Permeability Reservoirs Symposium, Denver, CO, April 15-17.
44. Madariage, M., et al.: "Integrated Petrophysical Model, C4 and C5 Reservoirs, VLA-6/9/21 Area, Block 1, Lagomar, Lake Maracaibo, Venezuela," paper SPE 69537 presented at the 2001 SPE Latin American and Caribbean Petroleum Engineering Conference, Buenos Aires, Argentina, March 25-28.
45. Marquez, L.J., et al.: "Improved Reservoir Characterization of a Mature Field Through an Integrated Multi-Disciplinary Approach: LL-04 Reservoir, Tia Juana Field, Venezuela," paper SPE 71355 presented at the 2001 SPE Annual Technical Conference and Exhibition, New Orleans, LA, Sept. 30-Oct. 3.
46. Marzouk, I., et al.: "New Classification of Carbonate Rocks for Reservoir Characterization," paper SPE 49475 presented at the 1998 SPE 8th Abu Dhabi International Petroleum Exhibition and Conference, Abu Dhabi, U.A.E., October 11-14.
47. Masters, J.A.: "Deep Basin Gas Trap, Western Canada," *AAPG Bull.*, v. 63 (1979), p.152-181.
48. Mathisen, T., Lee, S.H. and Datta-Gupta, A.: "Improved Permeability Estimates in Carbonate Reservoirs Using Electrofacies Characterization: A Case Study of the North Robertson Unit, West Texas," paper SPE 70034 presented at the 2001 SPE Permian Basin Oil and Gas Recovery Conference, Midland, TX, May 15-16.
49. Meyer, A., et al.: "The Upper Khuff Formation, Sedimentology, and Static Core Rock Type Approach Comparison of Two Offshore Abu Dhabi Fields," paper SPE 88794 presented at the 2004 11th Abu Dhabi International Petroleum Exhibition and Conference, Abu Dhabi, U.A.E., Oct. 10-13.
50. Montgomery, S., "East Texas Basin Bossier Gas Play" in *Petroleum Frontiers*, ed., J. Anderson, IHS Energy Group, Englewood, Colorado (2000), 1-60.
51. Morrow, N.R., Cather, M.E., and Buckley, J.S.: "Effects of Drying on Absolute and Relative Permeabilities of Low-Permeability Gas Sands," paper SPE 21880 presented at the SPE Rocky Mountain Regional Meeting and Low Permeability Reservoirs Symposium (1991), Denver, CO, April 15-17.
52. Neasham, J.W.: "Applications of Scanning Electron Microscopy to the Characterization of Hydrocarbon-Bearing Rocks," *Scanning Electron Microscopy* (1977a) vol. 7, 101-108.
53. Neasham, J.W.: "The Morphology of Dispersed Clay in Sandstone Reservoirs and Its Effect on Sandstone Shaliness, Pore Space and Fluid Flow Properties," paper SPE 6858 presented at the 52nd Annual Fall Technical Conference and Exhibition of the Society of Petroleum Engineers (1977b), October 9-12.
54. Neo, S., et al.: "Geological Framework Modeling and Rock Type Optimization for a Giant Oil Field, Offshore Abu Dhabi" paper SPE 49447 presented at the 1998 SPE 8th Abu Dhabi International Petroleum Exhibition and Conference, Abu Dhabi, U.A.E., Oct. 11-14.
55. Newsham, K.E. and Rushing, J.A.: "An Integrated Work-Flow Process to Characterize Unconventional Gas Resources: Part Geological Assessment and Petrophysical Evaluation," paper SPE 71351 presented at the SPE Annual Technical Conference and Exhibition (2001), New Orleans, LA, Sept. 30-Oct. 3.
56. Ohen, H.A., et al.: "Integrated Reservoir Study of Shushufindi Field Dynamic Modeling," paper SPE 89465 presented at the 2004 SPE/DOE Fourteenth Symposium on Improved Oil Recovery, Tulsa, OK, Apr. 17-21.
57. Pallatt, N., Wilson, J., and McHardy, B.: "The Relationship Between Permeability and the Morphology of Diagenetic Illite in Reservoir Rocks," *J. Pet. Tech.* (1984) 2225-2227.
58. Panesso, R., et al.: "Is It Possible to Reach a Detailed Upscaling From a Core-Old Logs Match? The Answer is Yes, If An Integrated Approach is Used. La Ceibita Field, Eastern Venezuela," paper SPE 69455 presented at the SPE Latin American and Caribbean Petroleum Engineering Conference (2001), Buenos Aires, Argentina, March 25-28.
59. Perez, H.H., Datta-Gupta, A., and Mishra, S.: "The Role of Electrofacies, Lithofacies, and Hydraulic Flow Units in Permeability Predictions from Well Logs: A Comparative Analysis Using Classification Trees," paper SPE 84301 presented at the SPE Annual Conference and Exhibition (2003), Denver, CO, October 5-8; *SPE Reservoir Evaluation and Engineering* (April 2005) 143-155.
60. Pittman, E.D. and Thomas, J.: "Some Applications of Scanning Electron Microscope to the Study of Reservoir Rock," *J. Pet. Tech.* (1979) 1375-1380.
61. Pittman, E.D., Larese, R.E., and Heald, M.T.: "Clay Coats: Occurrence and Relavence to Preservation of Porosity in Sandstones," in *Origin, Diagenesis, and Petrophysics of Clay Minerals in Sandstones: SEPM Special Publications* 47, D.W. Houseknecht and E.D. Pittman, eds. (1992a) 241-255.
62. Pittman, E.D.: "Relationship of Porosity and Permeability to Various Parameters Derived from Mercury Injection-Capillary Pressure Curves for Sandstone," *AAPG Bull.*, v. 76, no. 2 (1992b) 191-198.
63. Porras, J.C., Barbato, R., and Khazen, L.: "Reservoir Flow Units: A Comparison Between Three Different Models in the Santa Barbara and Pirital Fields, North Monagas Area, Eastern Venezuela Basin," paper SPE 53671 presented at the SPE Latin American and Caribbean Petroleum Engineering Conference (1999), Caracas, Venezuela, April 21-23.
64. Porras, J.C. and Campos, O.: "Rock Typing: A Key Approach for Petrophysical Characterization and Definition of Flow Units, Santa Barbara Field, Eastern Venezuela Basin," paper SPE 69458 presented at the SPE Latin American and Caribbean Petroleum Engineering Conference (2001), Buenos Aires, Argentina, March 25-28.
65. Purcell, W.R.: "Capillary Pressures—Their Measurement Using Mercury and the Calculation of Permeability Therefrom," *Trans. AIME*, v. 186 (1949).
66. Randolph, P.L., Soeder, D.J. and Chowdiah, P.: "Porosity and Permeability of Tight Sands," paper SPE/DOE/GRI 12836 presented at the SPE/DOE/GRI Unconventional Gas Recovery Symposium (1984), Pittsburgh, PA, May 13-15.

67. Rebelle, M., et al.: "Quantitative and Statistical Approach for a New Rock- and Log-Typing Model: Example of Onshore Abu Dhabi Upper Thamama," paper IPTC 10273 presented at the International Petroleum Technology Conference (2005), Doha, Qatar, November 21-23.
68. Rushing, J.A. and Newsham, K.E.: "An Integrated Work-Flow Process to Characterize Unconventional Gas Resources: Part Formation Evaluation and Reservoir Modeling," paper SPE 71352 presented at the SPE Annual Technical Conference and Exhibition (2001), New Orleans, LA, Sept. 30-Oct. 3.
69. Rushing, J.A., et al.: "Klinkenberg-Corrected Permeability Measurements in Tight Gas Sands: Steady-State versus Unsteady-State Techniques," paper SPE 89867 presented at the SPE Annual Technical Conference and Exhibition (2004), Houston, TX, Sept. 26-29.
70. Shenawi, S.H., et al.: "Permeability and Water Saturation Distribution by Lithologic Facies and Hydraulic Units: A Reservoir Simulation Study," paper SPE 105273 presented at the 15th SPE Middle East Oil & Gas Show and Conference (2005), Kingdom of Bahrain, March 11-14.
71. Soeder, D.J.: "Laboratory Drying Procedures and the Permeability of Tight Sandstone Core," *SPE Form. Eval.* (1986) 16-25.
72. Soto B., R., et al.: "Improved Reservoir Permeability Models from Flow Units and Soft Computing Techniques: A Case Study, Suria and Reforma-Libertad Fields, Columbia," paper SPE 69625 presented at the SPE Latin American and Caribbean Petroleum Engineering Conference (2001), Buenos Aires, Argentina, Mar. 25-28.
73. Stonecipher, S.A., Winn, R.D., Jr., and Bishop, M.G.: "Diagenesis of the Frontier Formation, Moxa Arch: A Function of Sandstone Geometry, Texture, Composition, and Fluid Flux," in *Clastic Diagenesis: AAPG Memoir 37*, D.A. McDonald and R.C. Surdam, eds. (1984) 289-316.
74. Stonecipher, S.A. and May, J.A.: "Facies Controls on Early Diagenesis: Wilcox Group, Texas Gulf Coast," in *Prediction of Reservoir Quality Through Chemical Modeling: AAPG Memoir 49*, I.D. Meshri and P.J. Ortoleva, eds. (1990) 25-44.
75. Swanson, B.F.: "A Simple Correlation Between Permeabilities and Mercury Capillary Pressure," *J. Pet. Tech.* (Dec. 1981) 2498-2504.
76. Thompson, A.H., Katz, A.J., and Rashke, R.A.: "Estimation of Absolute Permeability from Capillary Pressure Measurements," paper SPE 16794 presented at the 62nd Annual Technical Conference and Exhibition of the Society of Petroleum Engineers (1987), Dallas, TX, Sept. 27-30.
77. Varavur, S., et al.: "Reservoir Rock Typing in a Giant Carbonate," paper SPE 93477 presented at the SPE 14th Middle East Oil & Gas Show and Conference (2005), Bahrain, March 12-15.
78. Walls, J.D.: "Measurement of Fluid Salinity Effects on Tight Gas Sands with a Computer Controlled Permeameter," paper SPE 11092 presented at the SPE Annual Technical Conference and Exhibition (1982a), New Orleans, LA, Sept. 26-29.
79. Walls, J.D.: "Tight Gas Sands Permeability, Pore Structure, and Clay," *J. Pet. Tech.* (1982b) 2708-2714.
80. Wardlaw, N.C. and Taylor, R.P.: "Mercury Capillary Pressure Curves and the Interpretation of Pore Structure and Capillary Behavior in Reservoir Rocks," *Bull. Canadian Pet. Geol.*, v. 24, (1976).
81. Wilson, M.D. and Pittman, ED.: "Authigenic Clays in Sandstones: Recognition and Influence on Reservoir Properties and Paleoenvironmental Analysis," *J. Sed. Petrol.* (1977) v. 47, no. 1, 3-31.
82. Wilson, M.D.: "Origins of Clays Controlling Permeability and Porosity in Tight Gas Sands," *J. Pet. Tech.* (1982) 2871-2876.
83. Wilson, M.D.: "Non-Compositional Controls on Diagenetic Processes," in *Reservoir Quality Assessment and Prediction in Clastic Rocks: SEPM Short Course 30*, M.D. Wilson, ed. (1994) 183-208.